

A Survey on the Robustness of Computer Vision Models against Common Corruptions

Shunxin Wang, Raymond Veldhuis, Christoph Brune, Nicola Strisciuglio

Abstract—The performance of computer vision models are susceptible to unexpected changes in input images, known as common corruptions (e.g. noise, blur, illumination changes, etc.), that can hinder their reliability when deployed in real scenarios. These corruptions are not always considered to test model generalization and robustness. In this survey, we present a comprehensive overview of methods that improve the robustness of computer vision models against common corruptions. We categorize methods into four groups based on the model part and training method addressed: data augmentation, representation learning, knowledge distillation, and network components. We also cover indirect methods for generalization and mitigation of shortcut learning, potentially useful for corruption robustness. We release a unified benchmark framework (at <https://github.com/nis-research/CorruptionBenchCV>) to compare robustness performance on several datasets, and address the inconsistencies of evaluation in the literature. We provide an experimental overview of the base corruption robustness of popular vision backbones, and show that corruption robustness does not necessarily scale with model size. The very large models (above 100M parameters) gain negligible robustness, considering the increased computational requirements. To achieve generalizable and robust computer vision models, we foresee the need of developing new learning strategies to efficiently exploit limited data and mitigate unwanted or unreliable learning behaviors.

Index Terms—benchmark robustness, common corruptions, computer vision, model robustness



1 INTRODUCTION

1.1 Background and motivation

OVER the past decade, deep neural networks (DNNs) have been applied widely in many fields, such as face verification (e.g. banking [1], criminal tracking [2], border control [3]), autonomous driving [4], medical imaging [5] and computer-aided diagnoses [6], recommender systems [7], camera-based product quality monitoring [8]. In computer vision, DNNs are a core component of hallmark tasks such as object recognition [9] and detection [10], image segmentation [11], captioning [12], super-resolution [13], reconstruction [14], generation [15], and retrieval [16].

DNNs experience performance degradation in case of data distribution shifts, where the characteristics of test data differ from those of the training data [17]. For instance, a DNN-based diagnostic model trained on images captured in one hospital may not provide accurate diagnoses when applied to images from another hospital [18]. A doctor can instead make diagnoses based on images captured in different hospitals. This phenomenon becomes evident when DNNs trained on and that achieve high results on benchmark datasets are applied to real-world tasks. The observed degradation of performance poses a question about their reliability [19]. This aspect is not always considered in experimental evaluations and contrasts with what is experienced with the human visual system that robustly handles unexpected or unknown cases [20].

Studies on the robustness of DNNs for image classification have revealed that their performance is affected by three main factors, namely label noise [21], shortcut learning [22], and data distribution shifts [17].

Label noise occurs when an image is mislabeled in the ground truth. This negatively affects the effectiveness of

the models [23, 24, 25], as the incorrect label information provides confounding inputs to the DNNs during training [26, 27]. DNNs may overfit the label noise and consequently perform erroneous predictions [24].

Shortcut learning refers to DNNs exploiting simple solutions in the data instead of learning task-related semantic solutions. This might negatively impact the performance of models when tested on unseen data [22]. An example of shortcut learning is in Fig. 9a, where a text is embedded in images of a certain class [28]. The presence of the text in images of other classes leads to incorrect predictions, as it is learned to be the defining feature of that class.

Shortcut learning harms the robustness of DNNs: spurious correlations between images and labels may be misused as a backdoor, e.g. manually embedding shortcut features of a certain class to other classes results in errors.

Data distribution shifts can take various forms, e.g. adversarial noise [29] and common image corruptions [30]. Adversarial noise is visually imperceptible noise that impairs classification performance [29]. Common corruptions are caused by distortions like noise, blur or digital transformations that can occur during image collection or transmission [30]. Adversarial noise and image corruptions can cause significant performance degradation, and improving model robustness gained an increasing research interest [30, 31, 32, 33] (see Fig. 1).

1.2 Terminology

Common corruptions are visible distortions applied to images, causing a shift in data distribution from that of the original training data. Common corruptions in real scenarios include Gaussian noise, impulse noise, and defocus blur. Weather conditions also affect image quality, due to the presence

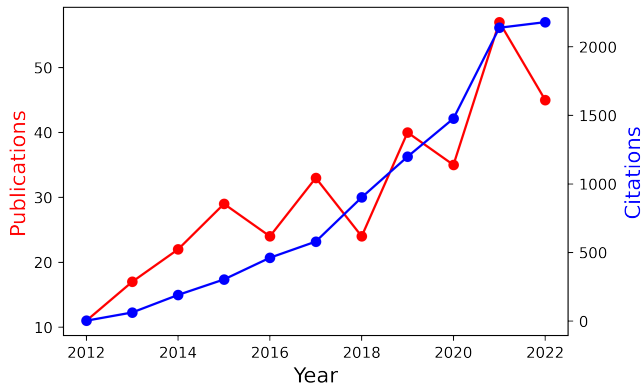


Fig. 1: The number of related publications to robustness to common image corruptions and the corresponding citation numbers from the year 2012 to 2022 (searched with keywords: ‘image corruption’, ‘corruption robustness’, ‘robustness to corruption’, excluding ‘label noise’ and ‘noisy labels’, and generated from Web of Science).

of fog, snow, etc. Examples from the ImageNet-C [30], ImageNet- \bar{C} [34], and ImageNet-3DCC [35] datasets are shown in Figs. 2b to 2d. Different from adversarial noise, image corruptions are visible transformations in images.

Corruption robustness refers to the ability of a computer vision model to withstand unexpected image corruptions occurring in the test samples, without significant degradation of performance. High corruption robustness means small performance degradation under image corruptions, to which the models generalize well. Note that the corruptions being tested should not be used for training, to ensure unbiased evaluation [30].

1.3 Contributions

We present a survey of research focused on improving the robustness of computer vision models to common corruptions that may be encountered by systems deployed in real-world scenarios. We focus on the period between 2012 and 2023, which has witnessed significant progress in this area. We collected and present results from relevant papers. As models are not evaluated in a complete and consistent way, we built a comprehensive benchmark suite for evaluating model performance on publicly available datasets. We benchmark the robustness of popular pre-trained backbones to common corruptions and provide a comprehensive analysis and unified comparison of their performance. By surveying the latest research in this area, we aim to 1) provide insights into effective approaches for improving the robustness of computer vision models against common corruptions, 2) identify areas for future research, and 3) contribute to the development of more robust and reliable computer vision systems that can operate effectively in real-world scenarios. Our contributions are as follows.

First, we present a comprehensive and systematic overview and taxonomy of works that characterize or improve the robustness of DNNs against common corruptions in computer vision. To the best of our knowledge, no other survey has focused on the corruption robustness of

computer vision models, providing a systematic taxonomy of methods, and a uniform comparison and analysis of different approaches. We aim to fill this gap in the literature, while Hendrycks *et al.* [30] instead provided benchmark metrics for evaluating corruption robustness. We categorize the methods for directly improving corruption robustness into four groups, namely: 1) data augmentation, 2) representation learning, 3) knowledge distillation, and 4) network component. We review also methods for improving generalization performance w.r.t. Out-of-Distribution (OOD) data and shortcut learning, which may also improve the corruption robustness of DNNs. We refer to these methods as indirect methods, and categorize them into four groups, i.e. 1) image restoration, 2) regularization, 3) robust optimization, and 4) shortcut learning mitigation.

Second, we benchmark relevant backbone networks for computer vision on the ImageNet-C, ImageNet- \bar{C} , ImageNet-3DCC, and ImageNet-P datasets. We investigate the robustness of different backbones against common corruptions, studying the impact of the complexity of network architecture and model size. The efforts made in this work for the unification of benchmark results provide a solid ground to analyze the pros and cons of different methods and summarize current research trends.

Third, we identify future research challenges and promising research directions related to improving corruption robustness. We contribute to making further steps toward the understanding of corruption robustness, generalization, and shortcut learning in computer vision.

The remainder of this paper is organized as follows. In Section 2, we describe other survey papers that focus on the robustness of DNNs against adversarial attacks and label noise. In Section 3, we introduce benchmark datasets and evaluation metrics. In Section 4, we provide a taxonomy of methods designed to explicitly address corruption robustness. We present an overview of the results of these methods (collected from the papers) and investigate the corruption robustness of different popular computer vision backbones (with a corruption robustness evaluation framework that we made publicly available) in Section 5. In Section 6, we introduce approaches that indirectly related to the robustness of computer vision models, and in Section 7, we discuss future challenges and opportunities for improving corruption robustness, followed by conclusions in Section 8.

2 RELATED WORKS

Survey papers about robust deep learning mostly focus on robustness against adversarial attacks and label noise. In this section, we provide an overview of existing surveys and discuss the evolution of their taxonomy over time.

2.1 Adversarial attacks and defenses.

DNNs are known to be vulnerable to small, imperceptible perturbations of their inputs, called adversarial attacks, which can lead to subtle misclassification. A comprehensive overview of different types of adversarial attacks and the corresponding defense methods was presented in [29]. The authors categorized adversarial attack scenarios based on (1)

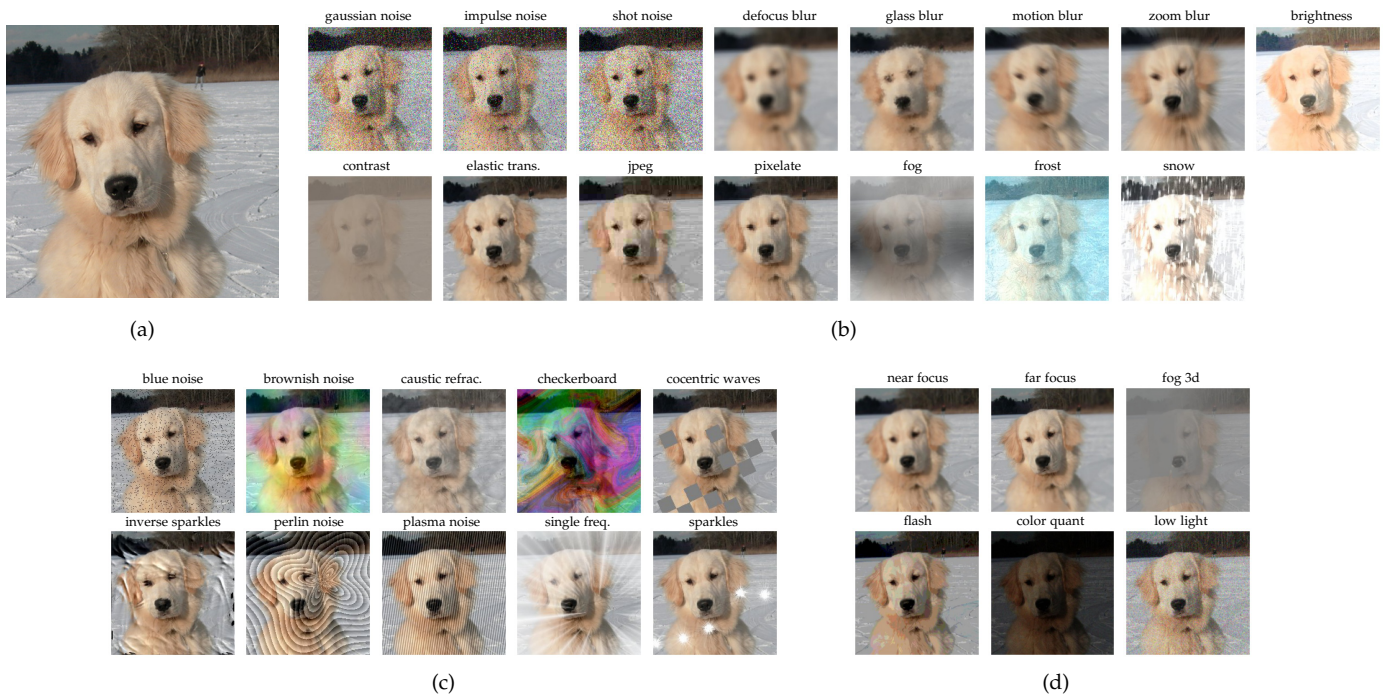


Fig. 2: (a) An image from ImageNet and its corrupted versions from (b) ImageNet-C, (c) ImageNet- \bar{C} (perceptually different from ImageNet-C), and (d) ImageNet-3DCC (using 3D information to improve realism).

when an attack happens (during training, testing, and application), (2) the prior knowledge of the target model (white-box or black-box attacks), and (3) the target of the attack (prediction confidence reduction, targeted or non-targeted misclassification). They further discussed defense methods and grouped them based on the way of implementation, including adversarial training, gradient hiding, defensive distillation, and feature squeezing. In [36], the authors further extended the categorizations of defense methods based on the work presented in [29], including gradient masking/obfuscation, robust optimization, and adversarial example detection. They mainly focused on methods for robust optimization including adversarial training, certified defenses, and regularization approaches. Different from model-agnostic common image corruptions, the generation of adversarial noise depends on the knowledge of a specific model. In [37], adversarial noise for training was shown to have a beneficial effect on the robustness of DNNs to common image corruptions.

2.2 Label noise

Label noise refers to the presence of incorrect ground truth labels that can mislead the training of DNNs, resulting in suboptimal model performance. The existence of label noise is hard to avoid since many datasets are labeled by non-experts or in a crowd-sourcing manner [38]. Additionally, some data contains ambiguous information, making it difficult even for experts to annotate correctly. The practice of training models on large-scale annotated datasets often involves the dependency on non-expert annotators (crowd-sourced labeling) [38] or pseudo labels created by the training models [39] to reduce the expensive cost of annotation.

These approaches result in an increase in label noise. Noisy labels are hard to recognize during training, and approaches to detect label noise and remove its influence are essential to improve the classification performance and robustness of DNNs. A taxonomy of label noise and its influence on the training of deep neural networks was presented in [21]. Different types of label noise were identified based on their statistical characteristics, i.e. the dependency on other variables such as the characteristics of certain classes. Label noise can have a significant impact on various aspects of a DNN, including classification performance, learning requirements, and model complexity and capacity. The methods reviewed in [5] to learn with label noise were grouped by implementation principles (e.g. ground truth label estimation and direct learning with label noise). New categories of robust methods against label noise were introduced in [40] (i.e. loss function and sample selection) and in [41] (i.e. sample weighting and meta-learning). The authors of [42] categorized the methods from a wider perspective (e.g. data modification, objective function, and optimization) than the previous surveys, and the categorization was further extended in [25] with extra groups like regularization and architecture modification.

These works presented an overview of methods for improving robustness toward adversarial attacks and label noise. However, an overview of methods for improving the robustness of computer vision models toward common image corruptions, with a unified analysis of their performance, is not yet available.

3 DATASETS AND METRICS

We review existing benchmark datasets to evaluate corruption robustness, adversarial robustness and OOD generalization (see Table 1 for an overview), and evaluation metrics.

3.1 Benchmark datasets for corruption robustness

Two benchmark datasets to evaluate and compare the corruption robustness, CIFAR-C and ImageNet-C, were proposed in [30]. The datasets were generated from the validation set of CIFAR and ImageNet respectively. CIFAR-C contains 19 synthetic corruptions while ImageNet-C contains 15 corruptions. There are four extra corruptions for ImageNet-C, which serve as a simplified corruption robustness validation set. Each corruption has five levels of severity. High severity indicates high strength of corruption applied to the original images. Fig. 2b shows the corruption types proposed in [30] with severity level equals to three.

The corruption types in CIFAR-C and ImageNet-C are insufficient to represent all the possible variations that can occur in the real world. Two complementary datasets, CIFAR- \bar{C} and ImageNet- \bar{C} were thus designed [34]. The set of corruptions included in these datasets contains the 10 most perceptually dissimilar corruptions to those of CIFAR-C and ImageNet-C (see Fig. 2c). To ensure realness, ImageNet-3DCC was designed, consisting of images generated by 3D corruptions that consider the scene geometry (see Fig. 2d) [35]. Thus, the resulting corruptions are more consistent with what may occur in the real world. For more data variety, Continuously Changing Corruptions (CCC) [43] combines pairs of corruptions to generate the corrupted images. Corruption types of varying severity and characteristics are combined through random walks to create a diverse set of benchmarks. To inspect how model predictions change as the effect of corruptions varies over time, time-dependent corruption sequences were generated in the CIFAR-P and ImageNet-P datasets [30]. Each frame of a sequence is corrupted based on its previous frame.

Although benchmark datasets are synthetically generated and may not cover all possible variations of corruptions that might occur in real-world scenarios, they still offer extensive ground for comparing the robustness of computer vision models. These datasets contain a wide range of corruption types, enabling the assessment of different aspects of robustness and generalization that are not typically evaluated when testing new algorithms and models. We thus contend that incorporating robustness testing into the performance evaluation of computer vision models should be a standard practice.

3.2 Benchmark datasets for adversarial robustness and OOD generalization

Adversarial robustness is also an essential aspect to assess computer vision models. In [46], two benchmark datasets named ImageNet-A and ImageNet-O were proposed. Both datasets contain naturally occurring adversarial images which are hard to recognize. ImageNet-O contains images of unknown classes while ImageNet-A contains images of known classes (seen during training). In [47], the authors proposed ImageNet-Patch, where an image contains adversarial patches that lead to degraded performance.

Examples of common datasets to test OOD generalization are OOD-CV [48], SI-Score [49], WILDS [50], and ImageNet-E [51]. They contain variations like pose, shape, texture, context, location, size, rotation, etc. Images with different renditions from the training data are considered OOD data as well. Typical datasets are ImageNet-R [31], ImageNet-D [44], ImageNet-Cartoon [45], and ImageNet-Drawing [45]. These datasets allow for measuring the generalization performance of models to different abstract renderings and the dependence of models on natural textures.

3.3 Evaluation metrics

3.3.1 Mean corruption and relative mean corruption error

Several metrics to measure corruption robustness were proposed in [30]. The mean corruption error (mCE) and relative corruption error (rCE) are basic metrics, computed as:

$$\text{mCE} = \frac{1}{|C|} \sum_{c \in C} \frac{\sum_{s=1}^5 E_{s,c}^f}{\sum_{s=1}^5 E_{s,c}^{\text{baseline}}}, \quad (1)$$

and

$$\text{rCE} = \frac{1}{|C|} \sum_{c \in C} \frac{\sum_{s=1}^5 (E_{s,c}^f - E_{s,c}^{\text{original}})}{\sum_{s=1}^5 (E_{s,c}^{\text{baseline}} - E_{s,c}^{\text{original}})}, \quad (2)$$

where C is the set of corruptions in the test set, $E_{s,c}^f$ is the classification error rate of a tested model f for a type of corruption c with severity s ranging from one to five, and baseline indicates the baseline model used for comparison. The mCE measures the classification performance of a model with respect to that of the baseline over all types of image corruption in the considered test set. When mCE is larger than one, the model f is less robust than the baseline model, and vice versa. The rCE measures the performance degradation of model f on corrupted images w.r.t. their original images, and compares it with that of the baseline model. Thus, a lower rCE value indicates better corruption robustness compared to the baseline model.

3.3.2 Mean flip rate

Mean flip rate (mFR) [30] was designed for the evaluation of the effects that consecutive corruptions have on the classification performance of models over time. It evaluates the probability of models changing their prediction across consecutive frames [30]. It is specifically used for image sequences having the same structure as those in ImageNet-P, where each sequence contains frames that are corrupted using the same type and level of corruption on top of the previous frame. The Flip Probability (FP) of the tested model f for the corruption c is computed as:

$$\text{FP}_c^f = \frac{1}{m(n-1)} \sum_{i=1}^m \sum_{j=2}^n \mathbb{1}(f(x_j^{(i)}) \neq f(x_{j-1}^{(i)})), \quad (3)$$

where m is the number of corruption sequences, n is the number of frames in a sequence, $x^{(i)}$ indicates the i^{th} sequence in the dataset and x_j indicates the j^{th} frame of a sequence. $\sum_{j=2}^n \mathbb{1}(f(x_j^{(i)}) \neq f(x_{j-1}^{(i)}))$ measures the number of frames in a sequence having different predictions from their previous frame, i.e. it compares the prediction of the model f on the frame x_j of the i^{th} sequence with that

TABLE 1: Benchmark datasets for data distribution shifts such as corruption, adversarial noise, rendition and OOD tests.

Category	Dataset	Image variation types
corruption	CIFAR-C [30]	Noise (Gaussian, Impulse, Shot, Speckle); Blur (Defocus, Glass, Gaussian, Motion, Zoom); Weather (Fog, Frost, Snow, Spatter); Digital (Brightness, Contrast, Elastic, Jpeg compression, Pixelate, Saturate)
	ImageNet-C [30]	Noise (Gaussian, Shot, Impulse); Blur (Defocus, Frosted glass, Motion, Zoom); Weather (Snow, Frost, Fog); Digital (Brightness, Contrast, Elastic, Pixelate, JPEG)
	CIFAR- \bar{C} [34]	Noise (Brown, Blue); Blur (Circular Motion Blur, Transverse Chromatic Aberration); Digital (Checkerboard, Lines, Inverse Sparkle, Sparkles, Pinch and Twirl, Ripple)
	ImageNet- \bar{C} [34]	Noise (Brown, Perlin, Blue, Plasma, Single Frequency, Concentric Sin Waves); Digital (Checkerboard, Caustic Refraction, Inverse Sparkle, Sparkles)
	CIFAR-P [30]	Noise (Gaussian, Shot); Blur (Motion, Zoom); Weather (Snow); Digital (Brightness, Rotate, Scale, Tilt, Translate)
	ImageNet-P [30]	Noise (Gaussian, Impulse, Shot, Speckle); Blur (Defocus, Glass, Gaussian, Motion, Zoom); Weather (Fog, Frost, Snow, Spatter); Digital (Brightness, Contrast, Elastic, Jpeg compression, Pixelate, Saturate)
	ImageNet-3DCC [35]	Noise (ISO, Low-light); Blur (Far focus, Near focus, XY-Motion, Z-Motion); Weather (Fog 3D); Digital (Bit Error, Color Quantization, Flash, CRF Compress, ABR Compress)
	CCC [43]	<i>Applied in random pairs:</i> Noise (Gaussian, Impulse, Shot, Speckle); Blur (Defocus, Glass, Gaussian, Motion, Zoom); Weather (Fog, Frost, Snow, Spatter); Digital (Brightness, Contrast, Elastic, Jpeg compression, Pixelate, Saturate)
rendition	ImageNet-D [44]	Real, Painting, Clipart, Sketch, Infograph and Quickdraw
	ImageNet-Cartoon [45]	ImageNet images converted to cartoon style
	ImageNet-Drawing [45]	ImageNet images converted to colored pencil drawings
	ImageNet-R [31]	Art, Cartoon, Graffiti, Line Drawing, Graphics, Origami, Painting, Pattern, Tattoo, Plastic Object, Plush Object, Video Game, Sculpture, Toy, and Embroidery
adversarial	ImageNet-A [46]	Adversarial noise exists in the collected samples
	ImageNet-O [46]	Adversarial noise exists in the collected samples
	ImageNet-Patch [47]	Adversarial patches
OOD	OOD-CV [48]	Shape, 3D pose, Texture, Context, and Weather
	SI-Score [49]	Shifted object size, Location, and Angle.
	WILDS [50]	Composed of 10 datasets with different modalities and sizes
	ImageNet-E [51]	Background, Size, Position, and Direction

on the previous perturbed images in the sequence. If the predictions are the same, $\mathbb{1}(f(x_j^{(i)}) \neq f(x_{j-1}^{(i)}))$ equals to zero, and the performance of the model is not affected by the considered corruptions. For a sequence corrupted by noise, the predictions are compared with those of the first frame, as noise is not temporally related. The mFR is obtained by averaging the flip rate FR_c^f across all the corruptions:

$$\text{mFR} = \frac{1}{|C|} \sum_{c \in C} \text{FR}_c^f = \frac{1}{|C|} \sum_{c \in C} \frac{\text{FP}_c^f}{\text{FP}_c^{\text{baseline}}}, \quad (4)$$

where C is the set of corruptions and FR_c^f is the standardized flip probability of the model f compared to that of the baseline model. The value of mFR is expected to be close to zero for a robust model.

3.3.3 Mean top-5 distance

Mean top-5 distance (mT5D) is also designed for ImageNet-P [30]. If a model is robust to the added corruptions, then the top-5 predictions of frames over a sequence should not be shuffled and should be relevant to those of the previous frames in the sequence. If the top-5 predictions are shuffled w.r.t. those of the previous frames in a sequence, the model should be penalized for its lack of robustness in maintaining accurate predictions under consecutive corruptions. The top-5 distance over each frame of m sequences belonging to a corruption c is:

$$\text{T5D}_c^f = \frac{1}{m(n-1)} \sum_{i=1}^m \sum_{j=2}^n d(\tau(x_j), \tau(x_{j-1})), \quad (5)$$

where $d(\tau(x_j), \tau(x_{j-1}))$ measure the deviation between the top-5 predictions of two consecutive frames, using:

$$d(\tau(x_j), \tau(x_{j-1})) = \sum_{i=1}^5 \sum_{j=\min\{i, \rho(i)\}+1}^{\max\{i, \rho(i)\}} \mathbb{1}(1 \leq j-1 \leq 5), \quad (6)$$

with

$$\rho(\tau(x_j)(k)) = \tau(x_{j-1})(k), \quad (7)$$

where $\tau(x_j)$ is the ranking of predictions for a corrupted frame x_j and $\tau(x_j)(k)$ indicates the rank of the prediction being k . If $\tau(x_j)$ and $\tau(x_{j-1})$ are identical, then $d(\tau(x_j), \tau(x_{j-1})) = 0$. Averaging the T5D normalized by that of the baseline over all corruptions corresponds to

$$\text{mT5D} = \frac{1}{|C|} \sum_{c \in C} \frac{\text{T5D}_c^f}{\text{T5D}_c^{\text{baseline}}}. \quad (8)$$

3.3.4 Relative and effective robustness

While mCE and rCE directly evaluate the corruption robustness, other metrics are designed to measure the OOD performance of DNNs and may indirectly reveal the corruption robustness of models. The *Relative Robustness* $\phi(f')$ [52] was proposed to compare directly the accuracy acc of a tested models f' with that of the baseline model f on the same dataset, computed as:

$$\phi(f') = acc_{\text{dataset}}(f') - acc_{\text{dataset}}(f). \quad (9)$$

A model with good relative robustness is expected to have a positive and high value of $\phi(f')$. The *Effective Robustness* $\epsilon(f')$ [52] was developed to compare the accuracy of a model tested on two different datasets, using:

$$\epsilon(f') = acc_{\text{dataset}_2}(f') - \beta(acc_{\text{dataset}_1}(f')), \quad (10)$$

where β is a function approximating the performance of different baseline models. It was empirically shown that the performance of the baseline models with different architectures on the original test set ($dataset_1$) and the distribution-shifted test set ($dataset_2$) fits a linear function. A positive high value of $\epsilon(f')$ indicates the model f' is more robust than the baseline models on $dataset_2$. However, this metric is impacted by the selection and training of the baseline models, bringing uncertainty to the evaluation process.

3.3.5 Expected calibration error

Instead of comparing models with a baseline, expected calibration error (ECE) [53] compares the accuracy and the confidence of the predictions, examining whether the models give reliable predictions. It is computed as:

$$ECE = \sum_{m=1}^M \frac{|B_m|}{n} |acc(B_m) - conf(B_m)|, \quad (11)$$

where M is the number of confidence interval bins separating the predictions, B_M is the samples in a confidence interval bin, n is the total number of samples in the test set, $acc(B_m)$ is the test accuracy on the set B_M while $conf(B_m)$ is the average confidence of the corresponding predictions. The lower the ECE, the more reliable the predictions.

4 METHODS FOR CORRUPTION ROBUSTNESS

We present a systematic overview of existing methods to improve corruption robustness and categorize them into four groups based on the part of the models considered and training methods. These categories include 1) data augmentation, 2) representation learning, 3) knowledge distillation, and 4) network component. The taxonomy is shown in Fig. 3. Since image corruption is a form of data distribution shifts, we also study methods addressing OOD generalization, as they might indirectly improve corruption robustness as a byproduct. However, these methods do not normally take corruption robustness into account for performance evaluation, but provide interesting ideas and insights that might inspire future works and strategies to unify robustness and generalization in computer vision. To differentiate from the methods targeting directly corruption robustness, we discuss the indirect approaches in Section 6.

4.1 Data Augmentation

Recent evidence suggests that the robustness of DNNs benefits enormously from well-annotated large-scale datasets since they contain more variations that might occur in the real world, filling the distribution gap between the training and test data [54, 52]. However, the cost of obtaining a large, well-annotated dataset can be excessively high. Thus, researchers synthetically generate data with different augmentations to increase data variety, bridging the distribution gap between training and testing data [33, 55]. This is shown to improve the corruption robustness of vision models [55].

Basic data augmentations. Basic data augmentations consist of simple transformations such as flipping, cropping, rotating, translation, color jittering, edge enhancement, etc [56]. Kernel filters are used to blur images, mimicking

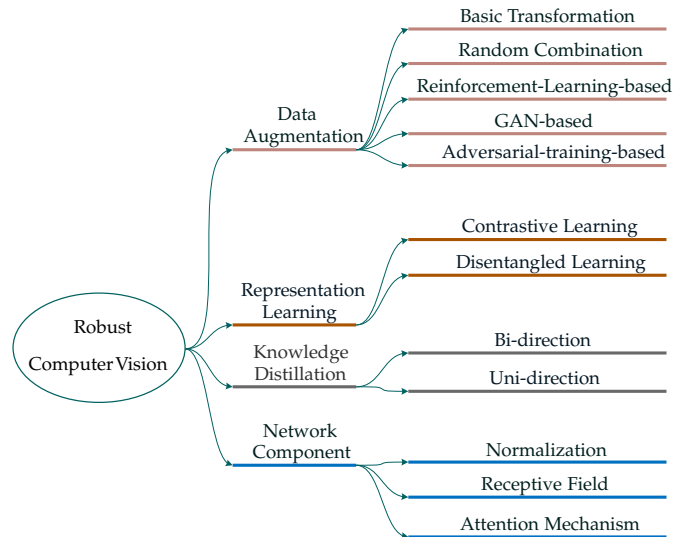


Fig. 3: Taxonomy of methods improving corruption robustness directly and indirectly.

motion blur, defocus blur, among others [57]. Pixel erasing removes pixels randomly from images [58], which is inspired by dropout regularization. Instead of augmenting an entire image, Patch Gaussian augmentation [59] applies Gaussian noise to small patches of images, which benefits the classification performance on both clean images and those affected by common image corruptions. For vision transformers, the authors of [60] proposed patch-based negative augmentation, including patch shuffling, rotation, and refill. The transformers are penalized if they perform well on patch-based augmented images, as this shows that they rely on local features in patches that are hard to recognize by human observers, rather than global structural features.

Advanced data augmentations. Combining different transformations can better increase data variety. Mixup [61] generates images by interpolating linearly two source images. The corresponding ground truth label of the interpolated images is also interpolated from the ground truth of the two images. Thus, a model is trained to predict linearly based on the weight of each source image in the interpolated versions, which improves robustness to label noise and adversarial samples. As an extension of Mixup, RobustMix [62] fuses the frequency bands of two images. The weight of each frequency band depends on its relative amount of energy. Thus, the models are regularized to classify based on low-frequency spatial features, which are more robust than high-frequency features [63], as they depend more on shapes rather than textures for classification [64].

LISA [65] aims at learning invariant predictors through selective augmentation, i.e. intra-label and intra-domain augmentations. Intra-label augmentation interpolates samples with the same labels but in different domains, learning useful semantics rather than spurious relations between domain information and the ground truth labels. Intra-domain augmentation instead interpolates samples with different labels but in the same domain. The learned representations can ignore unrelated domain information and focus on discriminative information to distinguish the samples.

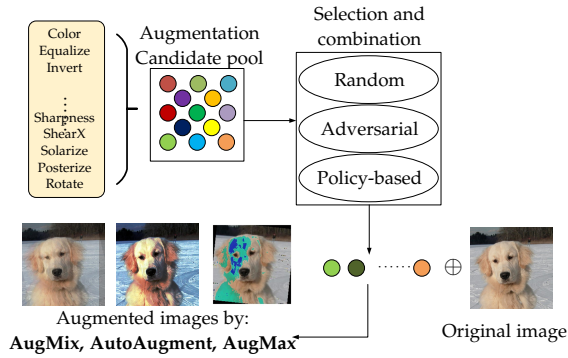


Fig. 4: Conceptual plot of automatic augmentation techniques. The selection and combination of the augmentations can be random, adversarial selected or policy-based.

Reinforcement learning was utilized in [66] to search for the best combination of augmentations, with a method called AutoAugment. However, the search process is computationally intensive and dataset-specific. Build on top of AutoAugment, the authors of [67] proposed adversarial Autoaugment, which learns adversarially to find augmentation policies. AugMix [33] augments images by randomly selecting augmentation operations. Jensen-Shannon divergence is applied to enforce the consistency of the augmented images (compared with the source image). Further, AugSVF [68] expands the options of possible transformations with additive Fourier-basis noise. Rather than randomly combining different augmentations, AugMax [69] adversarially selects augmentations and calculates the combined weights with back-propagation. PRIME [70] selects maximum-entropy image transformation, where the distributions of the chosen image transformations have maximum entropy. This guarantees that the complexity of samples reaches certain generalization bounds. Kim *et al.* [71] applied augmentations during test-time, which are selected by an auxiliary model that predicts suitable augmentations with low loss values. We provide a conceptual scheme of these automatic augmentation techniques in Fig. 4.

Targeted augmentation [72] is based on copy-paste, i.e. the object to be recognized is copied and pasted to different backgrounds, thus the predictive features that may vary across different backgrounds (domains) are preserved in the augmented images. This improves the generalization of models to OOD data, as it avoids learning the spurious correlation between backgrounds and the ground truth labels.

Generative-model-based. The above augmentations manipulate images directly. Augmentations can also be achieved by deep learning models, such as generative adversarial neural networks (GANs) [73, 74, 75, 76] and variational autoencoders (VAEs) [77]. Inspired by style transfer, where different augmentations can be considered as different domains, CycleGAN [76] utilizes a pair of autoencoders for bidirectional mapping, i.e. transferring an image from one domain to another. The cycle consistency loss ensures that images mapped back to the source domain are not contradictory to the source images, thus improving the quality of the generated images. It was used in [78, 79] to perform data

augmentation on medical images. Currently, model-based image generators aim at reducing data imbalance instead of improving corruption robustness. Although GANs and VAEs can generate an unlimited number of images with various levels of augmentation, the training process needs numerous computational resources and has high requirements of training data, when compared with basic augmentations. Moreover, the realness of the generated images needs more consideration, as it might affect the quality of training data.

Adversarial-training-based. Adversarial training forces computer vision models to classify images with (imperceptible) adversarial noise correctly [80]. Originally, it aimed at improving the adversarial robustness of computer vision models [81]. Subsequently, models trained adversarially are found to be as robust as biological neurons to adversarial perturbations [82], and adversarial training can help improve the robustness of models to common image corruptions, e.g. Gaussian adversarial training (GAT) [80] that enforces Gaussian distribution regularization to adversarial noise. A regularization term based on maximum entropy formulation is proposed in [83]. It encourages perturbing the source distribution of data rather than on the data directly. Thus, the generated adversarial samples bring more uncertainty to predictions. The work in [84] demonstrates that generating adversarial input patches for transformers improves their robustness against corruptions. Rather than directly adding noise to input, adversarial noise propagation (ANP) focuses on injecting noise to the hidden layers of NNs, which can be easily combined with other adversarial training methods [85]. Similarly, NoisyMix [86] applies augmentations in both input and feature space, making the decision boundary smoother. Diverse augmentation-based joint adversarial training (DAJAT) [87] further combines adversarial training with common augmentations, where two models are trained with augmented images and their source images respectively. The models share the same weights but with different statistics for batch normalization layers, being more robust to distribution shifts.

The commonality of these approaches is the target to improve corruption robustness by reducing the distribution difference between training and testing data, as the synthetically generated images increase data variety.

4.2 Representation learning

Robust representation learning aims at learning representations that are invariant to non-semantic changes in input images. The invariance constraint implicitly regularizes the models during training. Common ways to achieve this are contrastive learning [95, 90] and disentanglement learning [107]. They share the same idea to learn invariant semantics irrelevant to domain information by enforcing models to ignore domain-specific information. This can improve corruption robustness as the models learn to ignore the influence of corruptions.

Contrastive learning. Self-supervised learning is shown to be beneficial to improve the robustness of computer vision models [44, 92]. For instance, self-supervised contrastive learning [95] forces a model to learn similar latent representations for source images and their augmented versions, inducing the learning of representations that are invariant

TABLE 2: Overview of methods addressing corruption robustness, organized in four categories.

Category	Method	Codes	Remark
Data Augmentation	AutoAug. [66]	Yes	Apply reinforcement learning to learn the best augmentations
	Adv. AutoAug. [67]	No	Adversarial learning augmentation policies with reinforcement learning
	AugMix [33]	Yes	Combine augmentations randomly with JS-Divergence, ensuring consistency of images
	AugMax [69]	Yes	Adversarially select augmentations and their combined weights
	AugSVF [68]	No	Expands the options of operations in AugMix
	Mixup [61]	Yes	Linearly interpolate input examples and their ground truth
	Patch Neg. Aug. [60]	No	Transformers forced to predict incorrectly on shuffled, rotated, and infilled patches
	Gaussian Patch [59]	Yes	Small patches of Gaussian noise are added randomly
	RobustMix [62]	No	Frequency bands of input samples are mixed with energy-dependent weights
	Targeted Aug. [72]	No	Copy-paste the predictive features of images that may vary across different domains
	Adversarial Aug. [88]	No	Use adversarial noise in training
	RSPC [84]	Not yet	Reducing sensitivity to patch corruptions
	Test-time Aug. [71]	Yes	Augmentations to use are selected based on the characteristics of test data
	PRIME [70]	Yes	Augmentations with maximum entropy are selected during training
	Adv. Noise Propag. [85]	Yes	Adversarial noise is injected into hidden layers
	NoisyMix [86]	No	Apply adversarial noise in both input and feature space
	DAJAT [87]	Yes	Common augmentations combined with adversarial training
	ME-AdA [83]	Yes	Adversarial training with a maximum-entropy-based term to regularize the distribution of data
LISA [65]	Yes	intra-label or intra-domain augmentation	
L_p -AT [37]	Yes	L_p Adversarial Training	
GAT [80]	No	Gaussian noise generate adversarial examples	
Representation Learning	G-SimCLR [89]	Yes	Pseudo labels to avoid representation of the same category to be distant
	SupCon [90]	Yes	Ground truth labels to avoid representation of the same category to be distant
	Balanced-SupCon [91]	Yes	Apply InforNCE loss to avoid class collapse
	Self-learning [44, 92]	No	self-supervised learning for robust representations
	Percept.-similar [93]	No	Representations of perceptually similar images are learned to be similar
	Adv. Con [94]	Yes	Contrastive learning with adversarial noise
	SimCLR [95]	Yes	Self-supervised contrastive learning
CNC [96]	Yes	Contrastive learning helps mitigating learning spurious correlations	
Knowledge distillation	NoisyStudent [54]	Yes	A network trained on cleaned data teaches a student network trained on unlabeled data
	Auxiliary training [32]	Yes	Auxiliary classifier trained to predict corrupted data correctly, implicitly enforcing invariance
Robust Network Layer	AdaBN [97]	No	Adapt BN statistics to fit new dataset
	Push-pull Layer [98]	Yes	Biologically-inspired kernels result in robust response
	On-off Kernels [99]	Yes	Gaussian kernels with opposite directions
	Smoothing Kernel [100]	Yes	Kernel results in stabilized feature maps
	Winning hand [101]	No	Compressed networks from over-parameterized models
	LCANet [102]	Yes	Apply sparse coding layers in the front end
	ViT [103]	Yes	Vision transformer containing attention mechanism
	Patchifying Input [104]	Yes	Replacing down-sampling block by that of vision transformers
FAN [105]	Yes	Fully attentional networks considering self-attention and channel attention	
RVT [106]	Yes	Consist of robust building blocks e.g. patch embedding.	

to non-semantic changes. This improves the robustness of the model when the learned representations are used for downstream tasks like classification. In self-supervised contrastive learning, the images augmented from the same source image are called positive samples, while the rest are negative samples. The latent representations of the positive pairs are pulled together and the negative samples are pushed away from the positive samples (see Fig. 5). The authors in [93] use a perceptual similarity metric that mitigates the impact of irrelevant features on downstream tasks. The work in [94] combines adversarial training with contrastive learning. The problem with these methods is that the latent representations of the same class are also far away from each other, potentially influencing classification tasks, which need class-wise clustered representations. To avoid this, The authors of [89] additionally use k-means to generate pseudo

labels, which are then used to group images with different pseudo labels into the same batch during training.

Supervised contrastive learning (SupCon) [90] forces the image representations of the same class to be close to each other. Meanwhile, the representations of other classes are pulled away (see Fig. 5). However, this method requires a large batch size and thus the computational cost is high. It is also found that SupCon might result in class collapse, where all data samples of a class map to the same point in the latent space. Thus, an appropriate degree of spread of the representations of a certain class benefits the performance of models. Chen *et al.* [91] proposed a weighted class-conditional loss based on noise-contrastive estimation (InfoNCE [108]) to control the degree of spread. The loss helps better estimate the density of the distribution of positive samples, avoiding class collapse. As contrastive learning

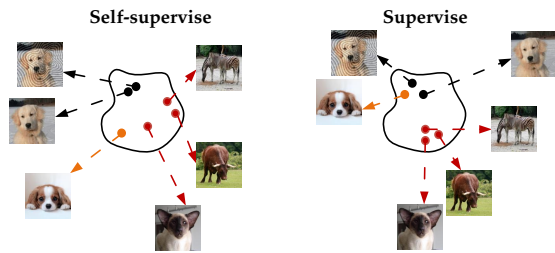


Fig. 5: Self-supervised [95] and supervised contrastive learning [90]. Without ground truth labels, self-supervised learning may result in learning representations of images from the same class far away from each other in the latent space. For supervised learning, although the image representations of the same class are closer in the latent space, this might result in class collapse when images from the same class point to the same representation.

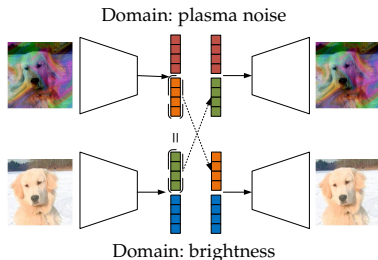


Fig. 6: In disentanglement learning, the representation of images is separated into two parts — style and content codes. The content code represents the semantics while the style code represents appearance and corruption information.

might be influenced by spurious correlation, where the learned representations do not completely catch meaningful semantics, a model based on empirical risk minimization (ERM) is used to predict spurious attributes, and its outputs are used to prepare positive and negative pairs [96].

Disentanglement learning. Disentanglement learning is useful for enforcing invariance to specific characteristics or properties of images in the latent space by separating the content code, which represents the semantics of an image, and the style code, which represents appearance or other factors related to the operational scenarios. As common corruptions are forms of style, disentangled representations allow for models to use the content codes only for tasks like classification. This improves the corruption robustness since the content codes are invariant to different corruptions. As illustrated in Fig. 6, the style and content codes are learned by cross-domain transfer. A pair of autoencoders is used to transfer images from a domain containing brightness to the other domain containing plasma noise. The content code extracted from the brightness domain together with the style code extracted from the plasma noise domain can be used to generate an image with plasma noise, and vice versa [107]. Being able to extract the content from different styles, models can be robust to different corruptions.

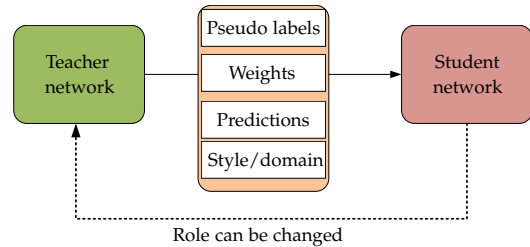


Fig. 7: General scheme of knowledge distillation. A student model can distill information from the teacher model, which can be pseudo labels [54], model weights [32], model predictions [32] or simulated domain/style information [109].

4.3 Knowledge distillation

Knowledge distillation helps the models identify misguided information or filter out meaningful information, thus contributing to increased generalization and corruption robustness. The framework of knowledge distillation needs at least two models: one as a teacher, and the other as a student, to distill information from one to another. To improve corruption robustness, the student model is set to distill invariant information w.r.t. image corruption from the teacher model. For instance, the auxiliary classifier in [32] assists the target model to learn invariant image representations regarding image corruptions. The target classifier is trained on original training images while the auxiliary classifier is trained on their augmented versions. Both classifiers share the same backbone, and the auxiliary classifier is trained to predict the same as the target classifier. Thus, the image representations of the original images and their augmented versions are close to each other in the latent space, ignoring the impact of image corruptions. Instead of supervised learning, NoisyStudent [54] trains models by semi-supervised learning. It requires large amounts of data and computational resources. The teacher model is trained on labeled data to provide pseudo labels for the student model. The student model is trained on a larger unlabelled dataset along with the pseudo labels provided by the teacher model. The roles of the teacher and student change in subsequent iterations: the student model becomes the teacher model, while the teacher becomes the student. It shows robustness to image corruptions as well as label noise. We provide a general scheme of knowledge distillation in Fig. 7. The student network can learn to distill information like pseudo labels, weights, predictions, and domain information from the teacher network, and their role can be exchanged during training.

4.4 Network component

The aim of designing robust network components is to reduce the impact of data distribution shifts, e.g. modifying the receptive field of filters in certain layers in neural networks [110, 111], normalizing the responses of intermediate layers [112, 113, 114], and applying attention mechanism which adjusts the learning of models from different parts of inputs [103, 106]. Thus, they are intrinsically robust to common corruptions.

Receptive field modification. Receptive field modification involves changing or extending the kernels of a layer, which

is often inspired by biological observations. A network with center blind-spot receptive fields is proposed in [110]. The noise in images is assumed to be pixel-wise independent, and thus the receptive field obtained from the pixels around can help reduce the influence of noise. Further, Laine *et al.* combine the receptive fields of a blind-spot network in four directions [111]. The network is robust to noise but not other corruptions. Motivated by the biological behavior of neurons in the human visual system, a push-pull layer is proposed in [98] and deployed as a substitute of convolutional layers [115]. It is based on a response inhibition that suppresses the response to noise and spurious texture. Similarly, the on-/off-kernels [99] are two Gaussian kernels following opposite directions and encourage excitatory center or inhibitory surround, which is shown to be beneficial to robustness under different illumination conditions. Spatial smoothing kernel [100] provides stabilized feature maps that might smooth the loss landscape. This work further explains the improved generalization of DNNs using global average pooling, ReLU6, and other similar techniques, as they have a similar effect on smoothing the responses of models. Recent works on sparse neural networks (SNNs) find that a compact model benefits corruption robustness, compared with its dense version [101, 116]. Instead of training an entire SNN, Locally Competitive Algorithm (LCANet) [102] uses sparse coding layers in the front end via lateral competition, which is inspired by a biological observation that neurons inhibit their neighboring neurons which have similar receptive fields.

Normalization layer. Normalization layers are originally designed to speed up the training process, by normalizing the distribution of the inputs of intermediate layers [112, 114, 113]. Subsequently, researchers showed that Batch Normalization (BN) layer improves the robustness of DNNs towards image corruptions [97], domain shift [117, 118], by simply rectifying the statistics of BN layer according to the new test data (Adaptive-BN). However, BN requires a batch of images to calculate the representative mean and variance. A single image is not enough to obtain representative statistics for the test data, limiting the deployment of Adaptive-BN in real applications. Instance normalization (IN) is originally designed to achieve better style transfer, where the feature maps are normalized using the mean and variance of each channel of each sample [114]. It was demonstrated in [119] that IN is robust to specific types of corruption (haze, fog, and smoke). Instead of normalizing in the spatial domain, convolutional normalization [120] performs normalization in the frequency domain of kernels of convolutional layers, which is shown to be robust to adversarial attacks and label noise.

Attention mechanism. Transformers have gained widespread application in computer vision over the past decade, for their outstanding accuracy in classification. What sets transformers apart from CNNs is their attention mechanism. This raises the question of whether the attention mechanism, in addition to achieving high accuracy, also benefits the robustness of models against common corruptions. The work of [121] investigated the robustness of transformers and found that the patch size of Vision Transformer (ViT) is important to robustness. Smaller patches were shown to benefit adversarial robustness.

Besides, they found that the robustness of ViTs against common corruptions does not differ much from that of ResNets. However, another study [103] demonstrated that self-attention mechanism improves the robustness of ViTs against common corruptions, compared to their CNN counterpart, BiT. Additionally, ViTs were found to be more robust to patch-wise corruptions and more susceptible to adversarial patches compared to CNNs [122]. Interestingly, patchifying images (replacing the downsampling block with the one used by ViT) is shown to benefit the corruption robustness of CNNs [104]. The authors in [106] uncovered that classification token (CLS) and locality constraints when calculating pair-wise attention among non-overlapping local patches impair robustness. Based on these findings, they design a new architecture using robust components like patch/position embedding, called Robust Vision Transformer (RVT). The work in [105] proposed fully attentional networks (FANs) which add a channel attention layer to improve the visual grouping of mid-level representations. Although several studies have shown that attention mechanisms can improve corruption robustness, more investigations are needed to obtain a comprehensive understanding of the capability of self-attention layer to enhance corruption robustness. This is because different works [121, 103, 122] reported inconsistent findings.

5 PERFORMANCE COMPARISON

Results collected from the literature are not always uniformed with respect to mCE, mFP, and mT5D, making it difficult to compare different works. We release a benchmark framework and evaluate the corruption robustness of relevant pre-trained backbones for computer vision. The benchmark addresses the current limitations of robustness tests that mostly focus, when considered in papers, on the ImageNet-C dataset, which does not cover broadly the test cases for corruption robustness of a model. Our framework uses a standardized set of benchmarks when evaluating model robustness, including ImageNet-C, ImageNet- \bar{C} , ImageNet-P, and ImageNet-3DCC. For the computation of mCE, mFP and mT5D, we use the same ResNet-18 baseline. We ensure that the results are comparable and that the evaluation is fair and unified across datasets and models. In the following, we also report results collected from the literature of methods addressing corruption robustness.

5.1 Pre-trained ImageNet-1k backbones

Evaluating model robustness to common corruptions is not usually performed when benchmarking new computer vision backbones. We conducted a thorough investigation of existing backbone models, with a new benchmark suite that includes metrics for evaluating corruption robustness on several datasets, such as ImageNet-C, ImageNet- \bar{C} , ImageNet-3DCC, and ImageNet-P¹. We used ImageNet-1k pre-trained ResNet-18 as the baseline model and report the results in Table 3 and Table 4. Our findings demonstrate the robustness of commonly used computer vision models when facing commonly corrupted images. The top-3 best

1. Codes will be made available with paper publication.

TABLE 3: Results of ImageNet-1k pre-trained backbone networks on ImageNet corruption benchmark datasets. The top-3 mCE/rCE (scaled by %) on each benchmark dataset are highlighted in bold and the best results of CNN and transformer are underlined (the lower the better). Baseline: ResNet-18.

Architecture	Networks	#Params (M)	ImageNet							
			C		\bar{C}		3DCC		P	
			mCE	rCE	mCE	rCE	mCE	rCE	mFP	mT5D
CNN	ResNet-50 [123]	25.56	91.17	107.9	92.63	112.18	91.5	106.99	65.64	109.39
	ResNet101 [123]	44.55	87.64	106.05	88.5	108.5	88.47	106.03	52.37	77.19
	ResNet152 [123]	60.193	87.1	106.1	88.48	108.65	88.09	108.41	49.53	71.79
	ResNeXt50 [124]	25.05	92.45	109.14	94.21	114.14	93.08	108.71	65.69	91.91
	ResNeXt101 [124]	126.89	86.45	105.42	86.93	107.07	88.07	106.65	46.29	66.83
	DenseNet121 [125]	7.98	93.96	102.21	95.67	106.83	94.33	101.24	76.86	92.91
	DenseNet161 [125]	28.681	92.16	102.78	94.09	106.02	93.23	104.92	64.07	79.71
	DenseNet201 [125]	20.014	93.04	103	94.36	105.3	93.97	104.89	67.32	82.09
	EfficientNet-B2 [126]	9.11	91.62	103.82	91.82	104.95	92.54	103.8	54.61	72.63
	EfficientNet-B4 [126]	19.342	88.19	100.54	87.7	96.39	89.72	99.68	47.05	<u>60.61</u>
	EfficientNet-B5 [126]	30.39	86.91	99.97	88.95	103.35	88.49	102.94	44.14	69.03
	CoatNet-nano [127]	15.14	89.52	102.61	89.43	103.95	92.06	105.25	63.6	87.06
	CoatNet-0 [127]	27.436	89.14	101.1	88.6	100.51	93.05	111.77	53.82	91.23
	CoAtNet-1 [127]	41.722	86.41	101.45	85.38	100.18	89	106.05	41.65	91.62
	ConvNext-T [128]	28.585	86.83	100.67	87.14	101.4	88.5	103.79	42.1	78.35
	ConvNext-B [128]	88.59	84.43	104.58	84.2	104.9	86.59	106.71	34.01	74.8
	ConvNext-L [128]	197.77	<u>83.74</u>	105.55	<u>83.26</u>	104.41	<u>85.68</u>	106.27	<u>30.20</u>	74.94
Transformer	Swin-S [129]	49.606	85.14	100.04	83.62	98.06	87.26	103.9	46.49	80.62
	Swin-B [129]	87.77	83.47	105.14	81.46	102.53	85.83	107.62	41.36	84.06
	Swin-L [129]	196.53	81.84	105.9	80.05	102.61	84.15	107.29	33.14	75.63
	VOLO-D3 [130]	86.33	83.65	106.91	84.72	109.7	85.12	108.03	29.84	55.55
	VOLO-D4 [130]	192.96	82.62	105.69	84.21	108.68	84.36	109.3	27.59	55.8
	VOLO-D5 [130]	295.46	82.44	106.24	83.68	109.24	84.24	107.89	26.44	54.95
	BEiTv2-B [131]	86.53	80.87	103.83	79.75	103.23	83.72	107.16	28.36	54.43
	BEiTv2-L [131]	304.43	<u>77.74</u>	102.55	77.06	102.02	80.69	106.08	19.93	43.68
	EdgeNeXt-S [132]	5.587	89.31	99.59	89.69	100.79	90.44	101.55	45.99	67.36
	EdgeNeXt-B [132]	18.51	86.17	105.7	87.02	108.07	87.76	106.93	32.17	57.47
	MViTv2-B [133]	51.47	83.34	104.16	81.82	102.37	85.71	106.65	36.52	81.25
	MViTv2-L [133]	217.993	81.85	103.36	81.18	99.07	84.26	108.09	32.18	76.97
	MaxVit-S [134]	68.928	84.27	101.35	82.46	98.98	86.3	105.17	36.84	87.33
	MaxVit-B [134]	119.468	83.41	101.19	81.78	99.11	85.77	105.55	34.84	96.24
	MaxVit-L [134]	211.786	83.23	101.02	81.46	98.73	85.6	105.4	33.49	97.04

mCE and rCE on ImageNet-C, ImageNet- \bar{C} , and ImageNet-3DCC, and the top-3 best mFP and mT5D on ImageNet-P, are highlighted in bold in Table 3.

Transformers have shown great potential in improving corruption robustness, as evidenced by the fact that the backbones with top-3 mCE, mFP and mT5D are based on transformers. Only one CNN, EfficientNet-B4, achieves one of the top-3 best rCE on ImageNet- \bar{C} and ImageNet-3DCC. Interestingly, ViT-L/16 with 304 million parameters and BEiTv2-B with 86 million parameters achieve similar mCE values on ImageNet-C and ImageNet-3DCC, indicating that corruption robustness does not scale with model size.

In Fig. 8, we analyze the relationship between the number of parameters and the mCE achieved by 32 backbones on the ImageNet-C, ImageNet- \bar{C} , and ImageNet-3DCC benchmarks. We observe that, for models with up to about 100 million parameters, the number of parameters and the mCE follow a linear relation (as shown by the blue lines in Fig. 8). Increasing the model size beyond a certain point does not necessarily guarantee a corresponding improvement in corruption robustness. The robustness gains for

models that have a parameter space larger than 100 million are indeed very small, despite their much larger complexity and training resources required.

Furthermore, we measured the reliability of predictions of these backbones by computing the average normalized ECE of models tested on ImageNet-C, ImageNet- \bar{C} , and ImageNet-3DCC in Table 4. The ECE of a pre-trained backbone is normalized by that of ResNet-18, by averaging per corruption type. An ECE value smaller than one indicates the predictions are more reliable than those of ResNet-18. Intriguingly, the transformers having superior mCE (e.g. ViT-L/16, BEiTv2-B, and BEiTv2-L) do not perform more reliable predictions than many CNNs (they have a much higher average normalized ECE than CNNs). The ECE of all the backbones is higher than one, showing that the reliability of the predictions given by the models is lower than that of ResNet-18, despite they have better accuracy on robustness tests. This suggests that progress on vision backbones requires focus to also address the robustness and generalization properties explicitly.

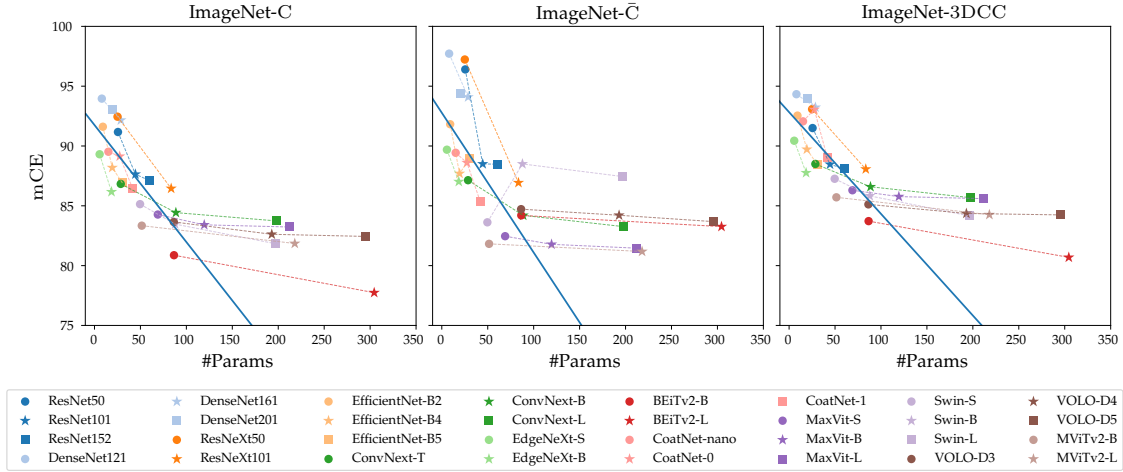


Fig. 8: The size of backbones versus mCE on ImageNet-C, ImageNet-C-bar, and ImageNet-3DCC. The mCE does not decrease linearly with an increase in model size. This demonstrates that a larger model is not an effective solution to improving corruption robustness, as the additional computational cost does not provide the expected benefits.

TABLE 4: Robustness reliability results of ImageNet-1k pre-trained backbones. The average normalized top-3 ECE on each benchmark dataset are in bold, while the best results of CNN and transformer are underlined. Baseline: ResNet-18.

Architecture	Networks	ImageNet			
		C	C-bar	3DCC	
CNN	ResNet-50 [123]	1.905	1.637	2.578	
	ResNet-101 [123]	1.502	<u>1.168</u>	1.735	
	ResNet-152 [123]	1.516	1.237	1.637	
	ResNeXt-50 [124]	2.008	1.841	2.366	
	ResNeXt-101 [124]	1.603	1.239	1.724	
	DenseNet-121 [125]	1.439	1.388	1.758	
	DenseNet-161 [125]	2.185	1.623	<u>1.438</u>	
	DenseNet-201 [125]	1.990	1.759	2.2	
	EfficientNet-B2 [126]	1.64	1.232	1.989	
	EfficientNet-B4 [126]	2.484	2.011	3.083	
	EfficientNet-B5 [126]	2.283	1.603	2.37	
	CoatNet-nano [127]	1.706	1.343	2.105	
	CoatNet-0 [127]	2.146	1.804	2.378	
	CoatNet-1 [127]	2.412	1.456	2.982	
	ConvNext-T [128]	2.097	1.665	2.803	
	ConvNext-B [128]	1.864	1.414	2.315	
	ConvNext-L [128]	2.172	1.496	2.308	
	Transformer	Swin-S [129]	1.942	1.526	2.359
		Swin-B [129]	1.473	1.151	1.66
		Swin-L [129]	1.759	1.425	2.805
VOLO-D3 [130]		2.835	1.922	2.758	
VOLO-D4 [130]		3.557	2.203	3.766	
VOLO-D5 [130]		3.692	2.37	3.421	
BEiTv2-B [131]		1.845	1.482	2.068	
BEiTv2-L [131]		1.669	1.187	1.83	
EdgeNeXt-S [132]		<u>1.172</u>	1.395	1.944	
EdgeNeXt-B [132]		1.521	1.297	1.727	
MViTv2-B [133]		1.594	1.211	1.768	
MViTv2-L [133]		2.249	1.531	2.657	
MaxViT-S [134]	1.579	1.095	1.747		
MaxViT-B [134]	1.653	1.127	1.852		
MaxViT-L [134]	1.499	1.093	1.542		

TABLE 5: Results of backbones distilling knowledge from or pre-trained on ImageNet-21k and tested on corruption robustness benchmarks. The top-3 results are in bold (the lower the better). Baseline: ResNet-18.

Networks	Params (M)	ImageNet				
		C	C-bar	3DCC	P	
		mCE	mCE	mCE	mFP	mT5D
Distillation BiT-50 [135]	25.55	86.3	85.62	88.43	45.74	68.80
BiT-50 [136]	25.55	92.85	93.79	94.62	88.95	94.84
BiT-101 [136]	44.541	91.24	92.02	92.95	79.84	87.59
BiT-152 [136]	936.533	89.32	89.8	91.12	70.21	93.48
Fine-tuning ViT-S/16 [137]	22.051	89.76	90.73	92	86.08	91.14
ViT-B/16 [137]	86.568	85.11	85.6	88.23	53.41	83.9
ViT-L/16 [137]	304.327	80.89	81.58	83.5	36.86	54.42

5.2 Fine-tuned and knowledge-distilled backbones

Fine-tuning models that are trained on large-scale datasets has been shown to improve the accuracy results [138]. Similarly, knowledge distillation trains models with a teacher model that distills meaningful information for a student model. We investigate further if fine-tuning or knowledge-distillation contributes to increasing corruption robustness. We test BiTs and ViTs with our benchmark framework and provide the results in Table 5. The first BiT-50 is trained with a teacher model that distills information from ImageNet-21k [138]. The other models are pre-trained on ImageNet-21k and then fine-tuned on ImageNet-1k.

Interestingly, pre-training on larger-scale datasets and fine-tuning on ImageNet-1K is not necessarily beneficial for corruption robustness, compared to using knowledge distillation. The fine-tuned BiT-50 has higher mCE than the distilled BiT-50. The fine-tuned BiT-101 and BiT-152 do not perform better than the distilled BiT-50 in terms of common corruptions robustness, despite their much larger capacity. The fine-tuned ViT-S/16 has a similar model size to the distilled BiT-50, but performs worse than it in terms of corruption robustness. Larger fine-tuned ViT-B/16 (86M parameters) and ViT-L/16 (304M parameters) achieved comparable

or better robustness than the distilled BiT-50, at the cost of much higher computational and memory requirements.

Note that, BiT-50 distilled knowledge from BiT-152, which is a large model. This demonstrates that proper utilization of large models needs better consideration, as we observe in the previous paragraphs that simply increasing model parameters does not necessarily gain more corruption robustness considering the efforts have been made. Other techniques that focus on data, e.g. methods that efficiently exploit available limited data, prior information, or large models during training, need further investigation.

5.3 Methods addressing corruption robustness

We collect the robustness results of existing approaches on the ImageNet-C benchmark datasets and report them in Table 6. Results on CIFAR-C are provided in Appendices. Most methods with benchmark results on ImageNet-C rely heavily on data augmentation techniques, while many methods from the other three categories do not follow a standard evaluation process to measure corruption robustness. For instance, they only use subsets of the available benchmarks. This highlights the need to establish a standardized evaluation procedure to ensure that models are tested consistently, allowing for a fair comparison of performance. Most of the robustness analyses of ImageNet-trained models are done solely on ImageNet-C, while other benchmark datasets such as ImageNet-C and ImageNet-3DCC are usually ignored.

Furthermore, different works may choose different baselines to compute the mCE, or report only the error rate of the models on the corruption benchmarks. As a result, the obtained values of mCE or other corruption robustness metrics are non-unified and sometimes non-directly comparable. In the following, we consider the error rate of models on ImageNet and ImageNet-C for comparison, as they are absolute values. NoisyStudent+EfficientNet-L2 [54] performs the best on ImageNet-C. Models with the second and third-best error rates are AdaBN+ResNeXt101 and AdaBN+DenseNet161 [97]. NoisyMix+ResNet-50 [86] has the fourth-best robust error rate. NoisyStudent [54] uses a dual-network architecture to extract useful information from millions of unlabelled images, which demands significant computational resources. The model was trained using augmentations that partially overlapped with those in ImageNet-C. As a result, it would be unfair to compare it directly with other models on this benchmark dataset.

Adaptive batch normalization layer [97] rectifies BN statistics that better fit the test data. The two models with the second and third-best error rates have a marginally large model size compared to those used by the augmentation-based methods. However, a major benefit of this method is its low computational requirements to rectify the statistics.

NoisyMix [86] performs data augmentation in both input and feature space. Thus, the complexity of the augmented training data is higher than those augmented by AugMax, thus gaining more improvement. This demonstrates that augmentation in feature space benefits corruption robustness and is worth more investigation.

These approaches commonly benefit from either large-scale training datasets or high-capacity models. However, as shown in Fig. 8, increasing model size alone does not

TABLE 6: The error rate on ImageNet (err) and the robust error rate (rerr) and mean corruption error (mCE scaled by %) on ImageNet-C. **ND** indicates ‘Not Disclose’.

Category	Method	err	rerr	mCE	baseline
Data augmentation	AugMix+SIN+ResNet-50 [33]	25.2	—	64.9	AlexNet
	AugMix+ResNet-50 [33]	22.4	—	68.4	AlexNet
	SIN+ResNet-50 [33]	27.2	—	73.3	AlexNet
	AutoAug.+ResNet-50 [33]	22.8	—	72.7	AlexNet
	AugMax+DuBIN+ResNet-18 [69]	32.38	64.99	82.56	AlexNet
	TestAug+ResNet-50 [71]	24.1	757	—	—
	PRIME+ResNet-50 [70]	23	45	57.5	ND
	RobustMix+ResNet-50 [62]	22.9	—	61.2	AlexNet
	AdA+All [88]	26.8	—	75.03	AlexNet
	AdA+Augmix+All [88]	28.32	—	72.27	AlexNet
	AdA+DeepAug.+All [88]	29.39	—	65.54	AlexNet
	NoisyMix+ResNet-50 [86]	22.4	47.7	—	—
Representation learning	RSPC+Swin-B [84]	17.2	—	45.7	AlexNet
	Patch-rotate+L2+ViT-B+ [60]	26.8	51.6	—	—
	SupCon+ResNet-50 [90]	—	—	67.2	AlexNet
Knowledge distillation	SupCon+ResNet-200 [90]	—	—	50.6	AlexNet
	Aux. training+ResNet-18 [32]	30.06	—	78.86	AlexNet
	Aux. training+ResNet-34 [32]	25.86	—	75.58	AlexNet
Network component	NS+EfficientNet-L2 [54]	11.6	22.2	28.3	AlexNet
	AdaBN+ResNet-18 [97]	—	58.2	73.7	AlexNet
	AdaBN+ResNet-50 [97]	—	51.3	64.9	AlexNet
	AdaBN+VGG-19 [97]	—	54.5	69.3	AlexNet
	AdaBN+ResNeXt-101 [97]	—	46.1	58.2	AlexNet
	AdaBN+DenseNet-161 [97]	—	45.3	57.4	AlexNet
	Patch4+ResNet-50-DW [104]	20.4	—	51.2	ND
	FAN-BiT-S-SA [105]	18.7	38.3	51.4	AlexNet
	RVT-B [106]	17.5	—	47.3	ND

guarantee a corresponding improvement in corruption robustness. Therefore, future research should focus on developing effective learning methods with limited data and computational resources.

6 INDIRECT APPROACHES

In this section, we review techniques that may improve corruption robustness, despite their evaluation process does not explicitly account for such robustness. We refer to them as indirect methods in this survey. Although these methods are not specifically designed to improve corruption robustness, they may provide valuable insights that are worth further investigation. Our focus is not on benchmarking these methods, but rather on providing a broader perspective on potential ways to improve corruption robustness. For instance, image restoration can improve image quality by removing the effect of corruptions, and thus models can have better performance on well-restored images. Regularization avoids overfitting, and robust optimization aims at optimizing the objective function under the worst-case. Both can improve the generalization performance of models, potentially improving corruption robustness. Shortcut learning mitigation encourages models to learn more task-related semantics, instead of the shortcut solutions in data. This might also benefit corruption robustness, as models learn to focus on meaningful semantics that is invariant to corruptions. Moreover, understanding the learning behavior of models might provide useful insights for designing methods addressing corruption robustness.

6.1 Image restoration

The first extensive and systematic benchmark of corruption robustness in image classification was proposed in 2019 [30], and earlier studies focused mostly on image restoration, e.g. image denoising [139]. To remove noise in an image, the basic approach is to smooth it with an average medium or Gaussian filter. However, the filtering causes the loss of high-frequency information which might be essential for recognition tasks [56]. An autoencoder can be trained to remove different corruptions with one network [139, 111]. To reconstruct images without corruption, pairs of corrupted and clean images are needed. The corrupted images are usually generated synthetically from the clean images, with fixed levels of noise. This causes the trained autoencoders to have limited adaptability to other noise levels and types than those used for training. To improve this, a feedback mechanism is used to generate images with different levels of noise during training [140]. This mechanism adjusts dynamically the noise level in the images, and thus the autoencoder is generalized to different levels of noise. The inconvenience of training denoising autoencoders is the prerequisite for clean and corrupted image pairs. An algorithm [139] for training an autoencoder with corrupted images only was able to remove photographic noise. However, it is based on a strong assumption that the noise is zero-mean, which may limit its applicability to a wider scope of cases. Based on this assumption, a non-local filtering layer [141] can extract the non-local self-similarity features of images, and generalize to different noise levels.

With a more complex training framework, MimicGAN [109] was designed to simulate corruptions in images by an auxiliary model and reconstruct the images without corruptions. The simulated corruptions are compared with true corruptions. With the latent representations including the corruption information, the latent representations without corruptions can be found in the manifold of a pre-trained GAN. However, the quality of the generated images is greatly limited by the performance of the GAN, and thus more exploration is needed to improve the image quality.

6.2 Regularization

Regularization can avoid overfitting and improve the generalization of DNNs. Thus, when testing on unseen corruptions, models trained with proper regularization techniques may show better robustness. The regularization techniques can be applied to three aspects: activation functions, weights of neural networks, and output distributions.

The activation regularization penalizes large activations and encourages small activations. It can encourage the networks to learn sparse representations with L_1 regularizer applied to the activations of layers [142]. For weight regularization, techniques like weight decay (L_1 or L_2 penalty) [143], dropout [144], and weight uncertainty [145] are used. Weight decay applies the L_1 or L_2 norm of weights as a penalty term in the objective function. It forces the networks to learn small weight values, reducing overfitting [143]. Despite adding a penalty term to objective functions, dropout [144] throws away some nodes of a NN randomly, making the model sparse and avoiding overfitting. Instead of regularizing the weight values, Bayesian Neural

Networks (BNNs) [145] bring uncertainty to the weights of neural networks by training an ensemble of models. The models learn the distributions of the weights. When the model is tested, its weights are sampled from the learned distribution. This improves the generalization of the DNNs on unknown data. For output regularization, Pereyra *et al.* [146] proposed a regularizer based on the entropy of the predictions of DNNs. A low entropy prediction indicates a reliable prediction. This can smooth the output distributions and eliminate sharp distributions. Wang *et al.* [147] focused on the outputs of intermediate layers and regularized their predictive power to avoid large impacts of local features on the predictions, by an extra classifier. It predicts the learned representations of the earlier layer at each location, resulting in a prediction map recording the prediction results. Thus, the map has the same size as the response of the earlier layer. Contrasting with the regular classifier in the network, the extra classifier is trained to predict wrongly. Therefore, the regular classifier pays more attention to global features, as the other classifier using local features has a negative impact on the predictions. The authors in [148] regularized the outputs of each layer in neural networks. For samples in the same categories, the model learns fewer peaky representations, resulting in smoother class boundaries and thus improving the generalization of models.

6.3 Robust optimization

Robust optimization (RO) aims at improving the robustness of decision-making models to uncertainty that might be caused by unexpected inputs [149], e.g. corrupted images. Among the RO techniques, distributionally robust optimization (DRO) minimizes the worst-case error to improve the model robustness to unknown OOD data [150, 151, 152]. In DRO, data collected from different environments is a prerequisite. Therefore, the worst-case error corresponds to the highest error of the model performing in one of the environments. The objective of the optimization is:

$$\arg \min_f \sup_{Q \in P(P_{tr})} E_{X, Y \sim Q} [l(f(X), Y)], \quad (12)$$

where f is the model, X is the data, Y is the ground truth label, l is the loss function, and $P(P_{tr})$ indicates the training sets with different data distributions. Due to the complexity of a convex optimization problem, the authors in [153] approximate the worst-case expected value through Bayesian optimization. Rather than optimizing the performance of a model in terms of the worst-case, invariance-based optimization (IBO) aims at finding the invariant information towards distribution shifts, with data collected from multiple environments [154, 155]. RO-based methods can improve the generalization of models to uncertain inputs, and it would be beneficial to investigate their contribution to corruption robustness.

6.4 Shortcut learning mitigation

Bias in data can affect how models use the data to achieve their tasks [156]. One example is shortcut learning. Shortcuts are simple solutions in data and harm the OOD generalization performance of models. They result from spurious

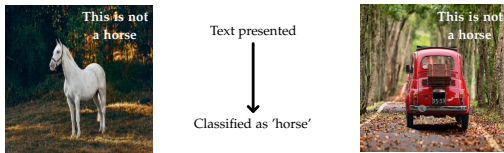


Fig. 9: Examples of shortcut learning: text embedded in training images of class ‘horse’ forms a spurious correlation between class ‘horse’ and the text, leading to incorrect predictions when the text is in an image of a car [28].

correlations between data and ground truth labels that ignore task-related semantics [22]. For instance, the embedded text in the images of class ‘horse’ induces the models to predict images with the text as a horse, even if the images do not contain horses (see Fig. 9a) [28]. The models do not generalize well to other images with horses but without the text. In another case, a model simply using a unique background color as a defining feature to predict a certain object lacks robustness to certain types of corruption that change the background of images.

Forcing models to learn more meaningful task-related semantics, shortcut learning mitigation is promising to improve generalization as well as corruption robustness. The authors in [157] first identify shortcuts in a medical image dataset, which are colored patches in images of benign cases. Then, they embedded similar colored patches in images of malignant cases. The networks learn to ignore the spurious correlations to the colored patches. Moreover, there might be visually unobservable shortcuts implicitly existing in data, e.g. frequency shortcut [158, 159] which is a specific small set of frequencies that corresponds to textures or shapes in the spatial domain and can be used to achieve classification for a certain class easily. However, the frequency-removal-based algorithm [158] can only provide a rough estimation of the learned frequency shortcuts. Thus, the explicit identification of imperceptible shortcuts is still challenging.

Without identifying the shortcuts, it could be difficult to mitigate their influence. To solve this, a regularization term [160] decoupling feature learning dynamics makes the identification of shortcuts unnecessary. During training, NNs learn from as many features as possible instead of a subset of features which minimizes cross-entropy loss. In [161], samples with a high shortcut degree distill less information to DNNs during training. The shortcut degree is measured by comparing the integrated gradients of prediction in terms of input at the early training stage and after training, because samples with shortcut features are preferred early in the training process. The approach is designed for Natural Language Understanding (NLU) models, but it can be also adapted to computer vision. For instance, instead of using the integrated gradient of predictions to evaluate shortcut degree, an auxiliary network with low capacity is used to identify the amount of shortcut information contained in images [162]. With the measured shortcut degree per training sample, the target network with high capacity can learn less from images with high shortcut degrees. The approach was shown to be feasible for synthetic shortcuts (e.g. a horizontal line and Gaussian

noise). Further investigation is needed for its feasibility for implicit shortcuts.

Dataset bias, as one of the reasons for shortcut learning, urges researchers to develop approaches targeting its mitigation. The work in [163] uses gradient-based scores to detect minority samples that induce bias, preventing the models from learning shortcut features caused by data bias.

Minderer *et al.* [164] proposed automatic shortcut removal in self-supervised representation learning. They utilized adversarial training to avoid NNs learning shortcut features like watermarks (e.g. when images of only one class have watermarks — a simple and common feature, NNs tend to use the feature for the classification of the class). The difference between adversarial perturbed images and the source images helps inspect the possibly learned shortcuts. The authors in [165] examined shortcut features in contrastive learning. They observe that the difficulty in distinguishing positive and negative images affects the predictability of extracted features. Implicit Feature Modification (IFM) [165] adds adversarial perturbations to the representations and allows models to learn from more predictive features without suppressing other good features. It outperforms state-of-the-art contrastive learning such as SimCLR [95] and Mocov2 [166]. But for simple tasks like color classification, the extracted features are complex and thus redundant. The definition of shortcut features needs more consideration instead of being limited to the complexity of extracted features. The methods addressing shortcut learning mitigation contribute to the understanding of the learning behavior of models. Although they are not designed to improve corruption robustness, they may provide a good inspiration for future work on robustness. For instance, one can design approaches to avoid unwanted learning behaviors that impair robustness.

7 CHALLENGES AND FUTURE OPPORTUNITIES

Corruption robustness is crucial for the deployment of computer vision models in safety-critical applications, e.g. autonomous-driving [4]. While there have been significant advances, several challenges and opportunities remain for improving the corruption robustness of these models. We discuss here some of these challenges and suggest possible directions for future research.

Coverage of potential corruption types and levels in the real world. One of the primary challenges in improving corruption robustness is extensively addressing corruption types and levels in real-world scenarios. The corruptions encountered in the real world can be more diverse than those included in the benchmark datasets, and a model may fail to generalize well to all these corruptions unseen during training. With limited data and computational resources, developing methods that can learn to handle a wide range of corruptions becomes critical. One way to address this challenge is to collect and annotate large-scale datasets that include diverse types of corruption. However, this is a time-consuming and expensive process. Augmentation-based approaches are currently the best solution, while the generation of synthetic corruptions needs further investigation to ensure the generated corruptions are sufficiently representative of real-world corruptions. This further supports future

research on developing methods that can effectively transfer knowledge from synthetic to real-world corruptions.

Investigation of architectures and training frameworks. While data augmentation is effective for improving corruption robustness, the other three categories of methods (representation learning, knowledge distillation, and network component) that focus on structural and architectural changes, need more investigation. Compared to augmentation-based methods which may overfit the robustness to corruptions seen during training, there are fewer methods and limited benchmark results for these approaches. Further investigation is required to improve the capability of these methods in learning robust representations that can be transferred to other tasks, distilling knowledge that is robust to corruptions, and being robust-by-design. These techniques are promising for improving model robustness and their potential benefits warrant further research to better understand their capabilities and limitations.

Effective training strategies with less computational resources. While large models and dataset size can benefit corruption robustness to some extent, the computational resources needed for training might not always be available. This could limit the reproducibility and usability of the methods. For instance, the backbone of NoisyStudent [54] has more than 480 million parameters and was trained using a vast amount of unlabelled images. Therefore, it is essential to develop efficient training strategies that can achieve the same level of corruption robustness with limited data and computational resources. This can involve techniques such as transfer learning [167], meta-learning [168], and few-shot learning [169], leveraging prior knowledge to learn from limited data. Transfer learning distills knowledge from one dataset to another. But distillation strategy needs to be properly designed, as we show that fine-tuning models pre-trained on a large-scale dataset does not necessarily guarantee better corruption robustness, but might have high standard accuracy. Meta-learning uses an outer algorithm to optimize e.g. the learning speed or the generalization performance of the inner algorithm, i.e. the target task. Few-shot learning aims at learning with few or zero samples by matching similar classes that are seen during training. With these methods, the limited data and computational resources can be used efficiently.

Potential of indirect methods to improve corruption robustness. Regularization and optimization approaches which focus on improving OOD generalization performance have the potential to improve corruption robustness. However, this is usually ignored in the performance evaluation procedure. Techniques to restore images from common corruptions directly improve image quality. While they only evaluate the image quality, how models can predict on these restored images is often overlooked. Therefore, future work on evaluating these techniques in terms of corruption robustness is needed.

Linking corruption robustness, OOD generalization, and shortcut learning mitigation. Corruption robustness and OOD generalization are closely related as common corruptions are a cause of data distribution shifts from the distribution of the training data. Shortcut learning, where a model relies on spurious correlations in the data to achieve high accuracy, can also impact corruption robustness. We find it

necessary to consider these three aspects when targeting the performance evaluation of models, and them to become part of standard practices in the performance evaluation process. The evaluation of robustness and generalization from multiple perspectives can yield more comprehensive and trustworthy results. Moreover, theoretical analysis that focuses on explaining the learning behavior of models [170, 171] and the factors guaranteeing OOD generalization [172] might help to better understand the intrinsic reasons for the impaired corruption robustness of computer vision models, potentially guiding the design of approaches for improving robustness. Regarding shortcut learning, it is important to develop methods that can identify and mitigate shortcut learning to provide a clearer understanding and evaluation of the generalization properties of models, and to enforce the learning of more task-related semantics.

Improving the corruption robustness of computer vision models is a challenging task, and requires the development of effective techniques that can handle diverse corruptions. In some cases, applications have hardware constraints on the site of training. Thus, designing robust methods that can operate with limited training data and computational resources is a promising direction to explore. Large-capacity models are not the best solution to guarantee corruption robustness, though they might achieve good performance on benchmarks. Smaller models can also be robust if they can distill proper knowledge from other models. Inducing bias [173] in the form of priors or expert knowledge is thus a promising direction. Future research should focus on investigating methods of all four categories, improving the connection among corruption robustness, OOD generalization, and shortcut learning mitigation. Achieving these goals will foster progress toward the safe and reliable deployment of computer vision models in real-world applications.

8 CONCLUSIONS

Corruption robustness is one crucial aspect of the performance evaluation of computer vision systems, as it indicates how well a model can operate in the presence of image corruption and provides insights into its effectiveness in challenging environments. We surveyed state-of-the-art techniques that address corruption robustness, including data augmentation, representation learning, knowledge distillation, and network component. As current benchmark results are not obtained in a unified and coherent way, we constructed a benchmark framework that allows for a unified evaluation of corruption robustness in computer vision. Using this framework, we evaluated popular pre-trained backbones. Transformers exhibit better corruption robustness than CNNs. Large model sizes improve corruption robustness, however, the degree of improvement in robustness does not always correspond with the size of the models, showing that **solely scaling up the models is not sufficient to ensure better corruption robustness**. Fine-tuning models pre-trained on large-scale datasets does not bring more corruption robustness than the model learned with knowledge distillation, demonstrating that **the knowledge transferred from large datasets needs specific design to benefit corruption robustness**. From the benchmark results collected from the literature, augmentation-based approaches are the

currently best approach to improve corruption robustness. We suggest focusing on efficient learning techniques that can work with limited computational resources and data, while also exploring the connection among corruption robustness, OOD generalization, and shortcut learning mitigation to gain deeper insight into the intrinsic mechanism and generalization abilities of models.

REFERENCES

- [1] G. Vishnuvardhan and V. Ravi, "Face recognition using transfer learning on facenet: Application to banking operations," in *Modern Approaches in Machine Learning and Cognitive Science: A Walkthrough: Latest Trends in AI, Volume 2* (V. K. Gunjan and J. M. Zurada, eds.), pp. 301–309, 2021.
- [2] S. T. Ratnaparkhi, P. Singh, A. Tandasi, and N. Sindhvani, "Comparative analysis of classifiers for criminal identification system using face recognition," in *2021 9th International Conference on Reliability, Infocom Technologies and Optimization (Trends and Future Directions) (ICRITO)*, pp. 1–6, 2021.
- [3] L. R. Carlos-Roca, I. H. Torres, and C. F. Tena, "Facial recognition application for border control," in *IJCNN*, pp. 1–7, 2018.
- [4] C. Chen, A. Seff, A. Kornhauser, and J. Xiao, "Deepdriving: Learning affordance for direct perception in autonomous driving," in *ICCV*, pp. 2722–2730, 2015.
- [5] J. Zhang, X. Wu, and V. S. Sheng, "Learning from crowdsourced labeled data: A survey," *Artificial Intelligence Review*, vol. 46, no. 4, p. 543–576, 2016.
- [6] C. Bhatt, I. Kumar, V. Vijayakumar, K. U. Singh, and A. Kumar, "The state of the art of deep learning models in medical science and their challenges," *Multimedia Systems*, vol. 27, no. 4, p. 599–613, 2020.
- [7] S. Zhang, L. Yao, A. Sun, and Y. Tay, "Deep learning based recommender system: A survey and new perspectives," *ACM Comput. Surv.*, vol. 52, feb 2019.
- [8] A. Kumar, "Computer-vision-based fabric defect detection: A survey," *IEEE Trans. Ind. Electron.*, vol. 55, no. 1, pp. 348–363, 2008.
- [9] M. Pak and S. Kim, "A review of deep learning in image recognition," in *CAIPT*, pp. 1–3, 2017.
- [10] L. Liu, W. Ouyang, X. Wang, P. Fieguth, J. Chen, X. Liu, and M. Pietikäinen, "Deep learning for generic object detection: A survey," *Int. J. Comput. Vis.*, vol. 128, pp. 261–318, 2020.
- [11] S. Minaee, Y. Boykov, F. Porikli, A. Plaza, N. Kehtarnavaz, and D. Terzopoulos, "Image segmentation using deep learning: A survey," *IEEE Trans. Pattern Anal. Mach. Intell.*, vol. 44, no. 7, pp. 3523–3542, 2022.
- [12] M. Stefanini, M. Cornia, L. Baraldi, S. Cascianelli, G. Fiameni, and R. Cucchiara, "From show to tell: A survey on deep learning-based image captioning," *IEEE Trans. Pattern Anal. Mach. Intell.*, vol. 45, no. 1, pp. 539–559, 2023.
- [13] Z. Wang, J. Chen, and S. C. H. Hoi, "Deep learning for image super-resolution: A survey," *IEEE Trans. Pattern Anal. Mach. Intell.*, vol. 43, no. 10, pp. 3365–3387, 2021.
- [14] H. B. Yedder, B. Cardoen, and G. Hamarneh, "Deep learning for biomedical image reconstruction: a survey," *Artificial Intelligence Review*, vol. 54, no. 1, pp. 215–251, 2020.
- [15] A. Figueira and B. Vaz, "Survey on synthetic data generation, evaluation methods and gans," *Mathematics*, vol. 10, no. 15, 2022.
- [16] S. R. Dubey, "A decade survey of content based image retrieval using deep learning," *IEEE Trans. Circuits Syst. Video Technol.*, vol. 32, no. 5, pp. 2687–2704, 2022.
- [17] Z. Shen, J. Liu, Y. He, X. Zhang, R. Xu, H. Yu, and P. Cui, "Towards out-of-distribution generalization: A survey," arXiv:2108.13624, 2021.
- [18] K.-H. Yu, A. L. Beam, and I. S. Kohane, "Artificial intelligence in healthcare," *Nature Biomedical Engineering*, vol. 2, pp. 719–731, 2018.
- [19] R. Geirhos, C. R. M. Temme, J. Rauber, H. H. Schütt, M. Bethge, and F. A. Wichmann, "Generalisation in humans and deep neural networks," in *NeurIPS*, vol. 31, 2018.
- [20] B. Recht, R. Roelofs, L. Schmidt, and V. Shankar, "Do ImageNet classifiers generalize to ImageNet?," in *ICML*, pp. 5389–5400, 2019.
- [21] B. Frenay and M. Verleysen, "Classification in the presence of label noise: A survey," *IEEE Trans. Neural Netw. Learn. Syst.*, vol. 25, no. 5, pp. 845–869, 2014.
- [22] R. Geirhos, J.-H. Jacobsen, C. Michaelis, R. Zemel, W. Brendel, M. Bethge, and F. A. Wichmann, "Shortcut learning in deep neural networks," *Nature Machine Intelligence*, vol. 2, pp. 665–673, nov 2020.
- [23] X. Zhu and X. Wu, "Class noise vs. attribute noise: A quantitative study," *Artificial Intelligence Review*, vol. 22, no. 3, pp. 177–210, 2004.
- [24] G. Algan and I. Ulusoy, "Image classification with deep learning in the presence of noisy labels: A survey," *Knowl Based Syst*, vol. 215, p. 106771, 2021.
- [25] H. Song, M. Kim, D. Park, Y. Shin, and J.-G. Lee, "Learning from noisy labels with deep neural networks: A survey," *IEEE Trans. Neural Netw. Learn. Syst.*, pp. 1–19, 2022.
- [26] D. Arpit, S. Jastrzebski, N. Ballas, D. Krueger, E. Bengio, M. S. Kanwal, T. Maharaj, A. Fischer, A. Courville, Y. Bengio, and S. Lacoste-Julien, "A closer look at memorization in deep networks," in *ICML*, pp. 233–242, 2017.
- [27] C. Zhang, S. Bengio, M. Hardt, B. Recht, and O. Vinyals, "Understanding deep learning requires rethinking generalization," in *ICLR*, 2017.
- [28] S. Lapsuchkin, S. Wäldchen, A. Binder, et al., "Unmasking Clever Hans predictors and assessing what machines really learn," *Nat Commun* 10, vol. 1096, 2019.
- [29] A. Chakraborty, M. Alam, V. Dey, A. Chattopadhyay, and D. Mukhopadhyay, "Adversarial attacks and defences: A survey," arXiv:1810.00069, 2018.
- [30] D. Hendrycks and T. Dietterich, "Benchmarking neural network robustness to common corruptions and perturbations," *Proceedings of the ICLR*, 2019.
- [31] D. Hendrycks, S. Basart, N. Mu, S. Kadavath, F. Wang, E. Dorundo, R. Desai, T. Zhu, S. Parajuli, M. Guo, D. Song, J. Steinhardt, and J. Gilmer, "The many faces of robustness: A critical analysis of out-of-distribution generalization," in *ICCV*, pp. 8340–8349, 2021.
- [32] L. Zhang, M. Yu, T. Chen, Z. Shi, C. Bao, and K. Ma, "Auxiliary training: Towards accurate and robust models," in *CVPR*, 2020.
- [33] D. Hendrycks, N. Mu*, E. D. Cubuk, B. Zoph, J. Gilmer, and B. Lakshminarayanan, "Augmix: A simple method to improve robustness and uncertainty under data shift," in *ICLR*, 2020.
- [34] E. Mintun, A. Kirillov, and S. Xie, "On interaction between augmentations and corruptions in natural corruption robustness," in *NeurIPS*, vol. 34, pp. 3571–3583, 2021.
- [35] O. F. Kar, T. Yeo, and A. Zamir, "3d common corruptions for object recognition," in *ICML 2022 Shift Happens Workshop*, 2022.
- [36] S. H. Silva and P. Najafirad, "Opportunities and challenges in deep learning adversarial robustness: A survey," arXiv:2007.00753, 2020.
- [37] K. Kireev, M. Andriushchenko, and N. Flammarion, "On the effectiveness of adversarial training against common corruptions," in *UAI*, pp. 1012–1021, 2022.
- [38] J. Zhang, X. Wu, and V. S. Sheng, "Learning from crowdsourced labeled data: a survey," *Artificial Intelligence Review*, vol. 46, pp. 543–576, 2016.
- [39] L. Jing and Y. Tian, "Self-supervised visual feature learning with deep neural networks: A survey," *IEEE Trans. Pattern Anal. Mach. Intell.*, vol. 43, no. 11, pp. 4037–4058, 2021.
- [40] N. Nigam, T. Dutta, and H. P. Gupta, "Impact of noisy labels in learning techniques: A survey," in *Advances in Data and Information Sciences*, pp. 403–411, 2020.
- [41] F. R. Cordeiro and G. Carneiro, "A survey on deep learning with noisy labels: How to train your model when you cannot trust on the annotations?," in *SIBGRAPI*, pp. 9–16, 2020.
- [42] B. Han, Q. Yao, T. Liu, G. Niu, I. W. Tsang, J. T. Kwok, and M. Sugiyama, "A survey of label-noise representation learning: Past, present and future," arXiv:2011.04406, 2020.
- [43] O. Press, S. Schneider, M. Kuehmerer, and M. Bethge, "CCC: Continuously changing corruptions," in *ICML 2022 Shift Happens Workshop*, 2022.
- [44] E. Rusak, S. Schneider, G. Pachitariu, L. Eck, P. V. Gehler, O. Bringmann, W. Brendel, and M. Bethge, "If your data distribution shifts, use self-learning," *Transactions on Machine Learning Research*, 2022.
- [45] T. Salvador and A. M. Oberman, "Imagenet-cartoon and imagenet-drawing: two domain shift datasets for imagenet," in

- ICML 2022 Shift Happens Workshop*, 2022.
- [46] D. Hendrycks, K. Zhao, S. Basart, J. Steinhardt, and D. Song, "Natural adversarial examples," in *CVPR*, pp. 15262–15271, 2021.
- [47] M. Pintor, D. Angioni, A. Sotgiu, L. Demetrio, A. Demontis, B. Biggio, and F. Roli, "Imagenet-patch: A dataset for benchmarking machine learning robustness against adversarial patches," *Pattern Recognition*, vol. 134, p. 109064, 2023.
- [48] B. Zhao, S. Yu, W. Ma, M. Yu, S. Mei, A. Wang, J. He, A. Yuille, and A. Kortylewski, "Ood-cv: A benchmark for robustness to out-of-distribution shifts of individual nuisances in natural images," in *ECCV 2022*, pp. 163–180, 2022.
- [49] J. Yung, R. Romijnders, A. Kolesnikov, L. Beyer, J. Djolonga, N. Houlsby, S. Gelly, M. Lucic, and X. Zhai, "SI-score: An image dataset for fine-grained analysis of robustness to object location, rotation and size," in *ICML 2022 Shift Happens Workshop*, 2022.
- [50] P. W. Koh, S. Sagawa, H. Marklund, S. M. Xie, M. Zhang, A. Balsubramani, W. Hu, M. Yasunaga, R. L. Phillips, I. Gao, T. Lee, E. David, I. Stavness, W. Guo, B. Earnshaw, I. Haque, S. M. Beery, J. Leskovec, A. Kundaje, E. Pierson, S. Levine, C. Finn, and P. Liang, "Wilds: A benchmark of in-the-wild distribution shifts," in *ICML*, pp. 5637–5664, 2021.
- [51] X. Li, Y. Chen, Y. Zhu, S. Wang, R. Zhang, and H. Xue, "Imagenet-e: Benchmarking neural network robustness via attribute editing," in *CVPR*, pp. 20371–20381, 2023.
- [52] R. Taori, A. Dave, V. Shankar, N. Carlini, B. Recht, and L. Schmidt, "Measuring robustness to natural distribution shifts in image classification," in *NeurIPS*, vol. 33, pp. 18583–18599, 2020.
- [53] C. Guo, G. Pleiss, Y. Sun, and K. Q. Weinberger, "On calibration of modern neural networks," in *ICML*, pp. 1321–1330, 2017.
- [54] Q. Xie, M. T. Luong, E. Hovy, and Q. V. Le, "Self-training with noisy student improves imagenet classification," in *CVPR*, pp. 10684–10695, 2020.
- [55] A. Robey, H. Hassani, and G. J. Pappas, "Model-based robust deep learning: Generalizing to natural, out-of-distribution data." arXiv:2005.10247, 2020.
- [56] C. Shorten and T. M. Khoshgoftaar, "A survey on image data augmentation for deep learning," *Journal of Big Data*, vol. 6, no. 1, p. 60, 2019.
- [57] G. Kang, X. Dong, L. Zheng, and Y. Yang, "Patchshuffle regularization." arXiv:1707.07103, 2017.
- [58] Z. Zhong, L. Zheng, G. Kang, S. Li, and Y. Yang, "Random erasing data augmentation," *AAAI*, vol. 34, no. 07, pp. 13001–13008, 2020.
- [59] R. G. Lopes, D. Yin, B. Poole, J. Gilmer, and E. D. Cubuk, "Improving robustness without sacrificing accuracy with patch gaussian augmentation." arXiv:1906.02611, 2019.
- [60] Y. Qin, C. Zhang, T. Chen, B. Lakshminarayanan, A. Beutel, and X. Wang, "Understanding and improving robustness of vision transformers through patch-based negative augmentation," in *NeurIPS 2021 Workshop on Distribution Shifts: Connecting Methods and Applications*, 2021.
- [61] H. Zhang, M. Cisse, Y. N. Dauphin, and D. Lopez-Paz, "mixup: Beyond empirical risk minimization," in *ICLR*, 2018.
- [62] J. Ngawne, M. A. NJIFON, J. Heek, and Y. Dauphin, "Robustmix: Improving robustness by regularizing the frequency bias of deep nets," in *NeurIPS 2022 Workshop on Distribution Shifts: Connecting Methods and Applications*, 2022.
- [63] H. Wang, X. Wu, Z. Huang, and E. P. Xing, "High-frequency component helps explain the generalization of convolutional neural networks," in *CVPR*, 2020.
- [64] R. Geirhos, P. Rubisch, C. Michaelis, M. Bethge, F. A. Wichmann, and W. Brendel, "Imagenet-trained CNNs are biased towards texture; increasing shape bias improves accuracy and robustness," in *ICLR*, 2019.
- [65] H. Yao, Y. Wang, S. Li, L. Zhang, W. Liang, J. Zou, and C. Finn, "Improving out-of-distribution robustness via selective augmentation," in *ICML*, pp. 25407–25437, 2022.
- [66] E. D. Cubuk, B. Zoph, D. Mane, V. Vasudevan, and Q. V. Le, "Autoaugment: Learning augmentation policies from data." arXiv:1805.09501, 2019.
- [67] X. Zhang, Q. Wang, J. Zhang, and Z. Zhong, "Adversarial autoaugment," in *ICLR*, 2020.
- [68] R. Soklaski, M. Yee, and T. Tsiligkaridis, "Fourier-based augmentations for improved robustness and uncertainty calibration," in *NeurIPS 2021 Workshop on Distribution Shifts: Connecting Methods and Applications*, 2021.
- [69] H. Wang, C. Xiao, J. Kossaifi, Z. Yu, A. Anandkumar, and Z. Wang, "Augmax: Adversarial composition of random augmentations for robust training," in *NeurIPS*, vol. 34, pp. 237–250, 2021.
- [70] A. Modas, R. Rade, G. Ortiz-Jiménez, S.-M. Moosavi-Dezfooli, and P. Frossard, "Prime: A few primitives can boost robustness to common corruptions," in *ECCV 2022*, pp. 623–640, 2022.
- [71] I. Kim, Y. Kim, and S. Kim, "Learning loss for test-time augmentation," in *NeurIPS*, vol. 33, pp. 4163–4174, 2020.
- [72] I. Gao, S. Sagawa, P. W. Koh, T. Hashimoto, and P. Liang, "Out-of-distribution robustness via targeted augmentations," in *NeurIPS 2022 Workshop on Distribution Shifts: Connecting Methods and Applications*, 2022.
- [73] T. Karras, S. Laine, and T. Aila, "A style-based generator architecture for generative adversarial networks," in *CVPR*, June 2019.
- [74] G. G. Chrysos, J. Kossaifi, and S. Zafeiriou, "Rocgan: Robust conditional gan," *Int. J. Comput. Vis.*, vol. 128, no. 10, pp. 2665–2683, 2020.
- [75] M. Mirza and S. Osindero, "Conditional generative adversarial nets." arXiv:411.1784, 2014.
- [76] J.-Y. Zhu, T. Park, P. Isola, and A. A. Efros, "Unpaired image-to-image translation using cycle-consistent adversarial networks," in *ICCV*, 2017.
- [77] J. P. Yun, W. C. Shin, G. Koo, M. S. Kim, C. Lee, and S. J. Lee, "Automated defect inspection system for metal surfaces based on deep learning and data augmentation," *Journal of Manufacturing Systems*, vol. 55, pp. 317–324, 2020.
- [78] M. Hammami, D. Friboulet, and R. Kechichian, "Cycle GAN-based data augmentation for multi-organ detection in ct images via yolo," in *ICIP*, pp. 390–393, 2020.
- [79] Z. Xu, C. Qi, and G. Xu, "Semi-supervised attention-guided cyclegan for data augmentation on medical images," in *2019 IEEE International Conference on Bioinformatics and Biomedicine (BIBM)*, pp. 563–568, 2019.
- [80] C. Yi, H. Li, R. Wan, and A. C. Kot, "Improving robustness of dnn against common corruptions via gaussian adversarial training," in *2020 IEEE International Conference on Visual Communications and Image Processing (VCIP)*, pp. 17–20, 2020.
- [81] A. Madry, A. Makelov, L. Schmidt, D. Tsipras, and A. Vladu, "Towards deep learning models resistant to adversarial attacks," in *ICLR*, 2018.
- [82] C. Guo, M. Lee, G. Leclerc, J. Dapello, Y. Rao, A. Madry, and J. Dicarlo, "Adversarially trained neural representations are already as robust as biological neural representations," in *ICML*, pp. 8072–8081, 2022.
- [83] L. Zhao, T. Liu, X. Peng, and D. Metaxas, "Maximum-entropy adversarial data augmentation for improved generalization and robustness," in *NeurIPS*, vol. 33, pp. 14435–14447, 2020.
- [84] Y. Guo, D. Stutz, and B. Schiele, "Improving robustness of vision transformers by reducing sensitivity to patch corruptions," in *CVPR*, pp. 4108–4118, 2023.
- [85] A. S. Liu, X. L. Liu, H. Yu, C. Z. Zhang, Q. Liu, and D. C. Tao, "Training robust deep neural networks via adversarial noise propagation," *IEEE TRANSACTIONS ON IMAGE PROCESSING*, vol. 30, pp. 5769–5781, 2021.
- [86] N. B. Erichson, S. H. Lim, W. Xu, F. Utrera, Z. Cao, and M. W. Mahoney, "Noisymix: Boosting model robustness to common corruptions." arXiv:2202.01263, 2022.
- [87] S. Addepalli, S. Jain, and V. B. R., "Efficient and effective augmentation strategy for adversarial training," in *NeurIPS*, vol. 35, pp. 1488–1501, 2022.
- [88] D. A. Calian, F. Stimberg, O. Wiles, S.-A. Rebuffi, A. György, T. A. Mann, and S. Goyal, "Defending against image corruptions through adversarial augmentations," in *ICLR*, 2022.
- [89] S. Chakraborty, A. R. Gosthipaty, and S. Paul, "G-simclr: Self-supervised contrastive learning with guided projection via pseudo labelling," in *2020 International Conference on Data Mining Workshops (ICDMW)*, pp. 912–916, 2020.
- [90] P. Khosla, P. Teterwak, C. Wang, A. Sarna, Y. Tian, P. Isola, A. Maschinot, C. Liu, and D. Krishnan, "Supervised contrastive learning," in *NeurIPS*, vol. 33, pp. 18661–18673, 2020.
- [91] M. Chen, D. Y. Fu, A. Narayan, M. Zhang, Z. Song, K. Fatahalian, and C. Re, "Perfectly balanced: Improving transfer and robustness of supervised contrastive learning," in *ICML*, pp. 3090–3122, 2022.
- [92] D. Hendrycks, M. Mazeika, S. Kadavath, and D. Song, "Using self-supervised learning can improve model robustness and uncertainty," in *NeurIPS*, vol. 32, 2019.
- [93] S. A. Taghanaki, K. Choi, A. H. Khasahmadi, and A. Goyal, "Ro-

- bust representation learning via perceptual similarity metrics," in *ICML*, pp. 10043–10053, 2021.
- [94] Z. Jiang, T. Chen, T. Chen, and Z. Wang, "Robust pre-training by adversarial contrastive learning," in *NeurIPS*, vol. 33, pp. 16199–16210, 2020.
- [95] T. Chen, S. Kornblith, M. Norouzi, and G. Hinton, "A simple framework for contrastive learning of visual representations," in *ICML*, pp. 1597–1607, 2020.
- [96] M. Zhang, N. S. Sohoni, H. R. Zhang, C. Finn, and C. Re, "Correct-n-contrast: a contrastive approach for improving robustness to spurious correlations," in *ICML*, pp. 26484–26516, 2022.
- [97] P. Benz, C. Zhang, A. Karjauv, and I. S. Kweon, "Revisiting batch normalization for improving corruption robustness," in *WACV*, pp. 494–503, 2021.
- [98] N. Strisciuglio, M. Lopez-Antequera, and N. Petkov, "Enhanced robustness of convolutional networks with a push-pull inhibition layer," *Neural Computing and Applications*, vol. 32, no. 24, pp. 17957–17971, 2020.
- [99] Z. Babaiee, R. Hasani, M. Lechner, D. Rus, and R. Grosu, "On-off center-surround receptive fields for accurate and robust image classification," in *ICML*, pp. 478–489, 2021.
- [100] N. Park and S. Kim, "Blurs behave like ensembles: Spatial smoothings to improve accuracy, uncertainty, and robustness," in *ICML*, pp. 17390–17419, 2022.
- [101] J. Diffenderfer, B. Bartoldson, S. Chaganti, J. Zhang, and B. Kailkhura, "A winning hand: Compressing deep networks can improve out-of-distribution robustness," in *NeurIPS*, vol. 34, pp. 664–676, 2021.
- [102] M. Teti, G. Kenyon, B. Migliori, and J. Moore, "LCANets: Lateral competition improves robustness against corruption and attack," in *ICML*, pp. 21232–21252, 2022.
- [103] S. Paul and P.-Y. Chen, "Vision transformers are robust learners," *AAAI*, vol. 36, no. 2, pp. 2071–2081, 2022.
- [104] Z. Wang, Y. Bai, Y. Zhou, and C. Xie, "Can CNNs be more robust than transformers?," in *ICLR*, 2023.
- [105] D. Zhou, Z. Yu, E. Xie, C. Xiao, A. Anandkumar, J. Feng, and J. M. Alvarez, "Understanding the robustness in vision transformers," in *ICML*, vol. 162, pp. 27378–27394, 2022.
- [106] X. Mao, G. Qi, Y. Chen, X. Li, R. Duan, S. Ye, Y. He, and H. Xue, "Towards robust vision transformer," in *CVPR*, pp. 12042–12051, 2022.
- [107] W. Du, H. Chen, and H. Yang, "Learning invariant representation for unsupervised image restoration," in *CVPR*, 2020.
- [108] A. van den Oord, Y. Li, and O. Vinyals, "Representation learning with contrastive predictive coding," 2019.
- [109] R. Anirudh, J. J. Thiagarajan, B. Kailkhura, and P.-T. Bremer, "Mimicgan: Robust projection onto image manifolds with corruption mimicking," *Int. J. Comput. Vis.*, vol. 128, pp. 2459–2477, 2020.
- [110] A. Krull, T.-O. Buchholz, and F. Jug, "Noise2void - learning denoising from single noisy images," in *CVPR*, 2019.
- [111] S. Laine, T. Karras, J. Lehtinen, and T. Aila, "High-quality self-supervised deep image denoising," in *NeurIPS*, vol. 32, 2019.
- [112] S. Ioffe and C. Szegedy, "Batch normalization: Accelerating deep network training by reducing internal covariate shift," in *ICML*, pp. 448–456, 2015.
- [113] Y. Wu and K. He, "Group normalization," in *ECCV*, 2018.
- [114] D. Ulyanov, A. Vedaldi, and V. Lempitsky, "Instance normalization: The missing ingredient for fast stylization." arXiv:1607.08022, 2017.
- [115] N. Strisciuglio and G. Azopardi, "Visual response inhibition for increased robustness of convolutional networks to distribution shifts," in *NeurIPS 2022 Workshop on Distribution Shifts: Connecting Methods and Applications*, 2022.
- [116] T. Chen, Z. Zhang, S. Liu, Y. Zhang, S. Chang, and Z. Wang, "Data-efficient double-win lottery tickets from robust pre-training," in *ICML*, pp. 3747–3759, 2022.
- [117] W.-G. Chang, T. You, S. Seo, S. Kwak, and B. Han, "Domain-specific batch normalization for unsupervised domain adaptation," in *CVPR*, 2019.
- [118] Y. Li, N. Wang, J. Shi, J. Liu, and X. Hou, "Revisiting batch normalization for practical domain adaptation," in *ICLR*, 2017.
- [119] Z. Xu, X. Yang, X. Li, and X. Sun, "The effectiveness of instance normalization: a strong baseline for single image dehazing." arXiv:1805.03305, 2018.
- [120] S. Liu, X. Li, Y. Zhai, C. You, Z. Zhu, C. Fernandez-Granda, and Q. Qu, "Convolutional normalization: Improving deep convolutional network robustness and training," in *NeurIPS*, vol. 34, pp. 28919–28928, 2021.
- [121] S. Bhojanapalli, A. Chakrabarti, D. Glasner, D. Li, T. Unterthiner, and A. Veit, "Understanding robustness of transformers for image classification," in *ICCV*, pp. 10231–10241, 2021.
- [122] J. Gu, V. Tresp, and Y. Qin, "Are vision transformers robust to patch perturbations?," in *ECCV 2022*, pp. 404–421, 2022.
- [123] K. He, X. Zhang, S. Ren, and J. Sun, "Deep residual learning for image recognition," in *CVPR*, 2016.
- [124] S. Xie, R. Girshick, P. Dollár, Z. Tu, and K. He, "Aggregated residual transformations for deep neural networks," in *CVPR*, 2017.
- [125] G. Huang, Z. Liu, L. van der Maaten, and K. Q. Weinberger, "Densely connected convolutional networks," in *CVPR*, 2017.
- [126] M. Tan and Q. Le, "EfficientNet: Rethinking model scaling for convolutional neural networks," in *ICML*, pp. 6105–6114, 2019.
- [127] Z. Dai, H. Liu, Q. V. Le, and M. Tan, "CoAtNet: Marrying convolution and attention for all data sizes," in *NeurIPS*, vol. 34, pp. 3965–3977, 2021.
- [128] Z. Liu, H. Mao, C.-Y. Wu, C. Feichtenhofer, T. Darrell, and S. Xie, "A convnet for the 2020s," in *CVPR*, pp. 11976–11986, 2022.
- [129] Z. Liu, Y. Lin, Y. Cao, H. Hu, Y. Wei, Z. Zhang, S. Lin, and B. Guo, "Swin transformer: Hierarchical vision transformer using shifted windows," in *ICCV*, pp. 10012–10022, 2021.
- [130] L. Yuan, Q. Hou, Z. Jiang, J. Feng, and S. Yan, "Volo: Vision outlooker for visual recognition," *IEEE Trans. Pattern Anal. Mach. Intell.*, vol. 45, no. 5, pp. 6575–6586, 2023.
- [131] H. Bao, L. Dong, S. Piao, and F. Wei, "BEit: BERT pre-training of image transformers," in *ICLR*, 2022.
- [132] M. Maaz, A. Shaker, H. Cholakkal, S. Khan, S. W. Zamir, R. M. Anwer, and F. Shahbaz Khan, "Edgenext: Efficiently amalgamated cnn-transformer architecture for mobile vision applications," in *ECCV 2022 Workshops*, pp. 3–20, 2023.
- [133] Y. Li, C.-Y. Wu, H. Fan, K. Mangalam, B. Xiong, J. Malik, and C. Feichtenhofer, "Mvitv2: Improved multiscale vision transformers for classification and detection," in *CVPR*, pp. 4804–4814, 2022.
- [134] Z. Tu, H. Talebi, H. Zhang, F. Yang, P. Milanfar, A. Bovik, and Y. Li, "Maxvit: Multi-axis vision transformer," in *ECCV 2022*, pp. 459–479, 2022.
- [135] L. Beyer, X. Zhai, A. Royer, L. Markeeva, R. Anil, and A. Kolesnikov, "Knowledge distillation: A good teacher is patient and consistent," in *CVPR*, pp. 10925–10934, 2022.
- [136] A. Kolesnikov, L. Beyer, X. Zhai, J. Puigcerver, J. Yung, S. Gelly, and N. Houlsby, "Big transfer (bit): General visual representation learning," in *ECCV 2020*, pp. 491–507, 2020.
- [137] A. Dosovitskiy, L. Beyer, A. Kolesnikov, D. Weissenborn, X. Zhai, T. Unterthiner, M. Dehghani, M. Minderer, G. Heigold, S. Gelly, J. Uszkoreit, and N. Houlsby, "An image is worth 16x16 words: Transformers for image recognition at scale," in *ICLR*, 2021.
- [138] T. Ridnik, E. Ben-Baruch, A. Noy, and L. Zelnik-Manor, "Imagenet-21k pretraining for the masses," in *NeurIPS, Datasets and Benchmarks Track*, 2021.
- [139] J. Lehtinen, J. Munkberg, J. Hasselgren, S. Laine, T. Karras, M. Aittala, and T. Aila, "Noise2noise: Learning image restoration without clean data," 2018.
- [140] R. Gao and K. Grauman, "On-demand learning for deep image restoration," in *ICCV*, pp. 1095–1104, 2017.
- [141] S. Lefkimmiatis, "Universal denoising networks : A novel cnn architecture for image denoising," in *CVPR*, pp. 3204–3213, 2018.
- [142] X. Glorot, A. Bordes, and Y. Bengio, "Deep sparse rectifier neural networks," in *AISTATS*, pp. 315–323, 2011.
- [143] A. Krogh and J. Hertz, "A simple weight decay can improve generalization," in *NeurIPS*, vol. 4, 1991.
- [144] N. Srivastava, G. Hinton, A. Krizhevsky, I. Sutskever, and R. Salakhutdinov, "Dropout: A simple way to prevent neural networks from overfitting," *J Mach Learn Res*, vol. 15, no. 56, pp. 1929–1958, 2014.
- [145] C. Blundell, J. Cornebise, K. Kavukcuoglu, and D. Wierstra, "Weight uncertainty in neural network," in *ICML*, vol. 37, pp. 1613–1622, 2015.
- [146] G. Pereyra, G. Tucker, J. Chorowski, Łukasz Kaiser, and G. Hinton, "Regularizing neural networks by penalizing confident output distributions," in *ICLR*, 2017.
- [147] H. Wang, S. Ge, Z. Lipton, and E. P. Xing, "Learning robust global representations by penalizing local predictive power," in *NeurIPS*, vol. 32, 2019.

- [148] C. Lassance, V. Gripon, and A. Ortega, "Laplacian networks: bounding indicator function smoothness for neural networks robustness," *APSIPA Transactions on Signal and Information Processing*, vol. 10, p. e2, 2021.
- [149] T. Tulabandhula and C. Rudin, "Robust optimization using machine learning for uncertainty sets." arXiv:1407.1097, 2014.
- [150] S. Sagawa*, P. W. Koh*, T. B. Hashimoto, and P. Liang, "Distributionally robust neural networks," in *ICLR*, 2020.
- [151] D. Bertsimas, V. Gupta, and N. Kallus, "Data-driven robust optimization," *Mathematical Programming*, vol. 167, pp. 235–292, 2018.
- [152] A. Setlur, D. Dennis, B. Eysenbach, A. Raghunathan, C. Finn, V. Smith, and S. Levine, "Bitrate-constrained DRO: Beyond worst case robustness to unknown group shifts," in *NeurIPS 2022 Workshop on Distribution Shifts: Connecting Methods and Applications*, 2022.
- [153] S. S. Tay, C. S. Foo, U. Daisuke, R. Leong, and B. K. H. Low, "Efficient distributionally robust Bayesian optimization with worst-case sensitivity," in *ICML*, pp. 21180–21204, 2022.
- [154] S. Chang, Y. Zhang, M. Yu, and T. Jaakkola, "Invariant rationalization," in *ICML*, vol. 119, pp. 1448–1458, 2020.
- [155] M. Koyama and S. Yamaguchi, "When is invariance useful in an out-of-distribution generalization problem?." arXiv:2008.01883, 2021.
- [156] N. Mehrabi, F. Morstatter, N. Saxena, K. Lerman, and A. Galstyan, "A survey on bias and fairness in machine learning," *ACM Comput. Surv.*, vol. 54, no. 6, 2021.
- [157] M. Nauta, R. Walsh, A. Dubowski, and C. Seifert, "Uncovering and correcting shortcut learning in machine learning models for skin cancer diagnosis," *Diagnostics*, vol. 12, no. 1, 2022.
- [158] S. Wang, R. Veldhuis, C. Brune, and N. Strisciuglio, "Frequency shortcut learning in neural networks," in *NeurIPS 2022 Workshop on Distribution Shifts: Connecting Methods and Applications*, 2022.
- [159] S. Wang, R. Veldhuis, C. Brune, and N. Strisciuglio, "What do neural networks learn in image classification? a frequency shortcut perspective," 2023.
- [160] M. Pezeshki, S.-O. Kaba, Y. Bengio, A. Courville, D. Precup, and G. Lajoie, "Gradient starvation: A learning proclivity in neural networks," in *NeurIPS*, 2021.
- [161] M. Du, V. Manjunatha, R. Jain, R. Deshpande, F. Deroncourt, J. Gu, T. Sun, and X. Hu, "Towards interpreting and mitigating shortcut learning behavior of NLU models," in *NAACL-HLT*, pp. 915–929, 2021.
- [162] N. Dagaev, B. D. Roads, X. Luo, D. N. Barry, K. R. Patil, and B. C. Love, "A too-good-to-be-true prior to reduce shortcut reliance," *Pattern Recognition Letters*, vol. 166, pp. 164–171, 2023.
- [163] S. Ahn, S. Kim, and S.-Y. Yun, "Mitigating dataset bias by using per-sample gradient," in *NeurIPS 2022 Workshop on Distribution Shifts: Connecting Methods and Applications*, 2022.
- [164] M. Minderer, O. Bachem, N. Houlsby, and M. Tschannen, "Automatic shortcut removal for self-supervised representation learning," in *ICML*, pp. 6927–6937, 2020.
- [165] J. Robinson, L. Sun, K. Yu, K. Batmanghelich, S. Jegelka, and S. Sra, "Can contrastive learning avoid shortcut solutions?," in *NeurIPS*, vol. 34, pp. 4974–4986, 2021.
- [166] K. He, H. Fan, Y. Wu, S. Xie, and R. Girshick, "Momentum contrast for unsupervised visual representation learning," in *CVPR*, 2020.
- [167] F. Zhuang, Z. Qi, K. Duan, D. Xi, Y. Zhu, H. Zhu, H. Xiong, and Q. He, "A comprehensive survey on transfer learning," *Proceedings of the IEEE*, vol. 109, no. 1, pp. 43–76, 2021.
- [168] T. Hospedales, A. Antoniou, P. Micaelli, and A. Storkey, "Meta-learning in neural networks: A survey," *IEEE Trans. Pattern Anal. Mach. Intell.*, vol. 44, no. 9, pp. 5149–5169, 2022.
- [169] Y. Song, T. Wang, S. K. Mondal, and J. P. Sahoo, "A comprehensive survey of few-shot learning: Evolution, applications, challenges, and opportunities." arXiv:2205.06743, 2022.
- [170] H. Shah, K. Tamuly, A. Raghunathan, P. Jain, and P. Netrapalli, "The pitfalls of simplicity bias in neural networks," in *NeurIPS*, vol. 33, pp. 9573–9585, 2020.
- [171] P. Izmailov, P. Kirichenko, N. Gruver, and A. G. Wilson, "On feature learning in the presence of spurious correlations," in *NeurIPS*, vol. 35, pp. 38516–38532, 2022.
- [172] R. Xu, X. Zhang, Z. Shen, T. Zhang, and P. Cui, "A theoretical analysis on independence-driven importance weighting for covariate-shift generalization," in *ICML*, vol. 162, pp. 24803–24829, 2022.
- [173] A. Goyal and Y. Bengio, "Inductive biases for deep learning of higher-level cognition," *Proc. R. Soc. A: Math. Phys. Eng. Sci.*, vol. 478, no. 2266, 2022.

APPENDIX A

ROBUSTNESS RESULTS ON CIFAR

Most papers that report benchmark results on CIFAR-C present methods for improved model robustness based on data augmentation, similarly to the case of ImageNet-related experiments.

In Table 7, we report and compare the error rate achieved by models on the CIFAR-10/100 datasets. We observed that CARD+LRR+WideResNet-18 [101] (from the category: network component) achieved the lowest error rate on both datasets. This approach involves complex algorithms for learning a sparse neural network, which results in a compressed model size but increases the training time significantly. AugMax+ResNeXt29 [69], which augments images with adversarially selected augmentations, achieved the second-lowest error rate.

Among the augmentation-based approaches, AugMax [69] performed the best on both the original test set of CIFAR and its corrupted versions, with the lowest error rate. AugMax selects augmentations randomly and combines them with weights computed adversarially, leading to the worst-case of mixtures. This is why it performs better than AugMix and AutoAugment, where augmentations and combination weights are sampled randomly or learned, respectively. Although using adversarial noise during training can improve the corruption robustness [37, 80], augmentations using spatial transformations contribute to more outstanding improvements, as demonstrated by e.g. AugMix [33] and AugMax [69].

TABLE 7: Results on CIFAR-10/100 and CIFAR-10/100-C. The **err** stands for the error rate on the original test set, **robust err** indicates the error rate on the corrupted versions and **mCE** is the mean corruption error. **ND** indicates ‘Not disclose’.

Category	Method	CIFAR-10			CIFAR-100			baseline
		err	robust err	mCE (%)	err	robust err	mCE (%)	
Data augmentation	AugMix+AllConvNet [33]	—	15	—	—	42.7	—	—
	AugMix+DenseNet [33]	—	12.7	—	—	39.6	—	—
	AugMix+WideResNet [33]	—	11.2	—	—	35.9	—	—
	AugMix+ResNeXt [33]	—	10.9	—	—	34.9	—	—
	AutoAugment+AllConvNet [33]	—	29.2	—	—	55.1	—	—
	AutoAugment+DenseNet [33]	—	26.6	—	—	53.9	—	—
	AutoAugment+WideResNet [33]	—	23.9	—	—	49.6	—	—
	AutoAugment+ResNeXt [33]	—	24.2	—	—	51.3	—	—
	Adv. Training+AllConvNet [33]	—	28.1	—	—	56	—	—
	Adv. Training+DenseNet [33]	—	27.6	—	—	55.2	—	—
	Adv. Training+WideResNet [33]	—	26.2	—	—	55.1	—	—
	Adv. Training+ResNeXt [33]	—	27	—	—	54.4	—	—
	Mixup+AllConvNet [33]	—	24.6	—	—	53.4	—	—
	Mixup+DenseNet [33]	—	24.6	—	—	55.4	—	—
	Mixup+WideResNet [33]	—	22.3	—	—	50.4	—	—
	Mixup+ResNeXt [33]	—	22.6	—	—	51.4	—	—
	AugSVF+WideResNet [68]	5.2	9.9	—	24.9	34.8	—	—
	AugMax+ResNet18 [69]	4.24	9.64	—	21.31	34.25	—	—
	AugMax+WRN40-2 [69]	4.32	9.33	—	23.2	33.65	—	—
	AugMax+ResNeXt29 [69]	3.61	7.89	—	19.3	31.14	—	—
	AdA+EDSR [88]	—	—	15.47	—	—	—	ND
	AdA+EDSR+AugMix [88]	—	—	9.4	—	—	—	ND
	AdA+EDSR+AugMix+DeepAugment [88]	—	—	7.83	—	—	—	ND
	ME-ADA+AllConvNet [83]	—	21.8	—	—	48.8	—	—
	ME-ADA+DenseNet [83]	—	23.1	—	—	52.2	—	—
	ME-ADA+WideResNet [83]	—	16.7	—	—	47.2	—	—
	ME-ADA+ResNeXt [83]	—	16.6	—	—	42.7	—	—
	ANP+VGG16 [85]	—	8.3	75.7	—	—	—	VGG16
	Gaussian patch+ResNet18 [32]	4.87	—	63.17	—	—	—	AlexNet
	Gaussian patch+WRN50 [32]	4.34	—	66.63	—	—	—	AlexNet
	Gaussian patch+ResNeXt50 [32]	4.48	—	66.63	—	—	—	AlexNet
	GAT+WRN-40-2 [80]	5.9	14.6	—	25.6	40.7	—	—
	GAT+AugMix+WRN-40-2 [80]	4.7	9.9	—	24.5	34.6	—	—
Test-time-Aug-k-2-Flip + Wide-ResNet [71]	—	—	—	—	32.6	—	—	
PRIME+ResNet18 [70]	5.8	10.2	10.2	21.6	31.8	31.8	ND	
DAJAT-Base-2*AA + WRN-34-10 [87]	11.29	19.88	—	31.25	43.05	—	—	
L_∞ -AT + ResNet18 [37]	6.7	17.3	—	—	—	—	—	
L_2 -AT + ResNet18 [37]	6.4	16.6	—	—	—	—	—	
Representation learning	Self-sup (rotation)+WRN-40-2 [92]	—	23.1	—	—	—	—	
	ACL(DS)+ResNet18 [94]	17.81	47.18	—	—	—	—	
Knowledge distillation	Auxiliary training + ResNet18 [32]	3.98	—	57.01	20.53	—	69.34 AlexNet	
	Auxiliary training + Wide-ResNet50 [32]	3.51	—	55.41	19.16	—	68.89 AlexNet	
	Auxiliary training + ResNeXt50 [32]	3.66	—	49.37	18.49	—	69.13 AlexNet	
Network component	AdaBN+ResNet20 [97]	—	27	90.7	—	55.5	87.4 AlexNet	
	AdaBN+ResNet56 [97]	—	18.6	63	—	52	81.9 AlexNet	
	AdaBN+ResNet18 [97]	—	15.7	53	—	—	AlexNet	
	AdaBN+ResNet50 [97]	—	16.9	57.6	—	—	AlexNet	
	AdaBN+VGG19 [97]	—	19	63.7	—	48.6	76.6 AlexNet	
	AdaBN+ResNeXt29 [97]	—	14.5	49.9	—	34	53.7 AlexNet	
	AdaBN+DenseNet [97]	—	12.4	42.4	—	34.2	54.2 AlexNet	
	Push-pull+ResNet56 [98]	—	26.33	91	—	—	AlexNet	
	Push-pull+DenseNet100-24 [98]	—	21.37	73	—	—	AlexNet	
CARD+LRR+WideResNet-18 [101]	3.2	7.25	—	19.4	28.7	—	AlexNet	

APPENDIX B

DETAILED ROBUSTNESS RESULTS OF PRE-TRAINED IMAGENET BACKBONES

In Figs. 10 to 18, we provide a detailed performance comparison of pre-trained backbones against different common ImageNet-based corruptions. Counter-intuitively, increasing model size to enhance model robustness against common corruptions is not an effective approach, especially for corruptions like Brownish noise, Perlin noise, near focus, far focus, 3D-fog, JPEG compression, color quantization, bit error, h265 abbreviation, elastic transform, caustic refraction, sparkles, and brightness. We observe that for these corruptions, large model size does not contribute to reduce the mean corruption error mCE and increase the accuracy, different from the effect that it has on other corruptions. Moreover, for models with parameter count higher than about 100M, the gain in robustness saturates, highlighting that the notable increase of complexity and memory requirements does not translate into generalization and robustness improvement.

B.1 Robustness against noise corruptions

Fig. 10 and Fig. 11 report the performance of pre-trained backbones on different noise corruptions. Interestingly, from the average normalized ECE values, we observe that large models provide less reliable predictions compared to those of small models, except in the case plasma noise corruption is present. Small transformers (e.g. VOLO-D3 and MViTv2-B) are more robust to plasma noise than the others. This is because plasma noise contains colors warped in different ways, which might just affect the average intensity of small image patches, and thus the small transformers are more robust to it.

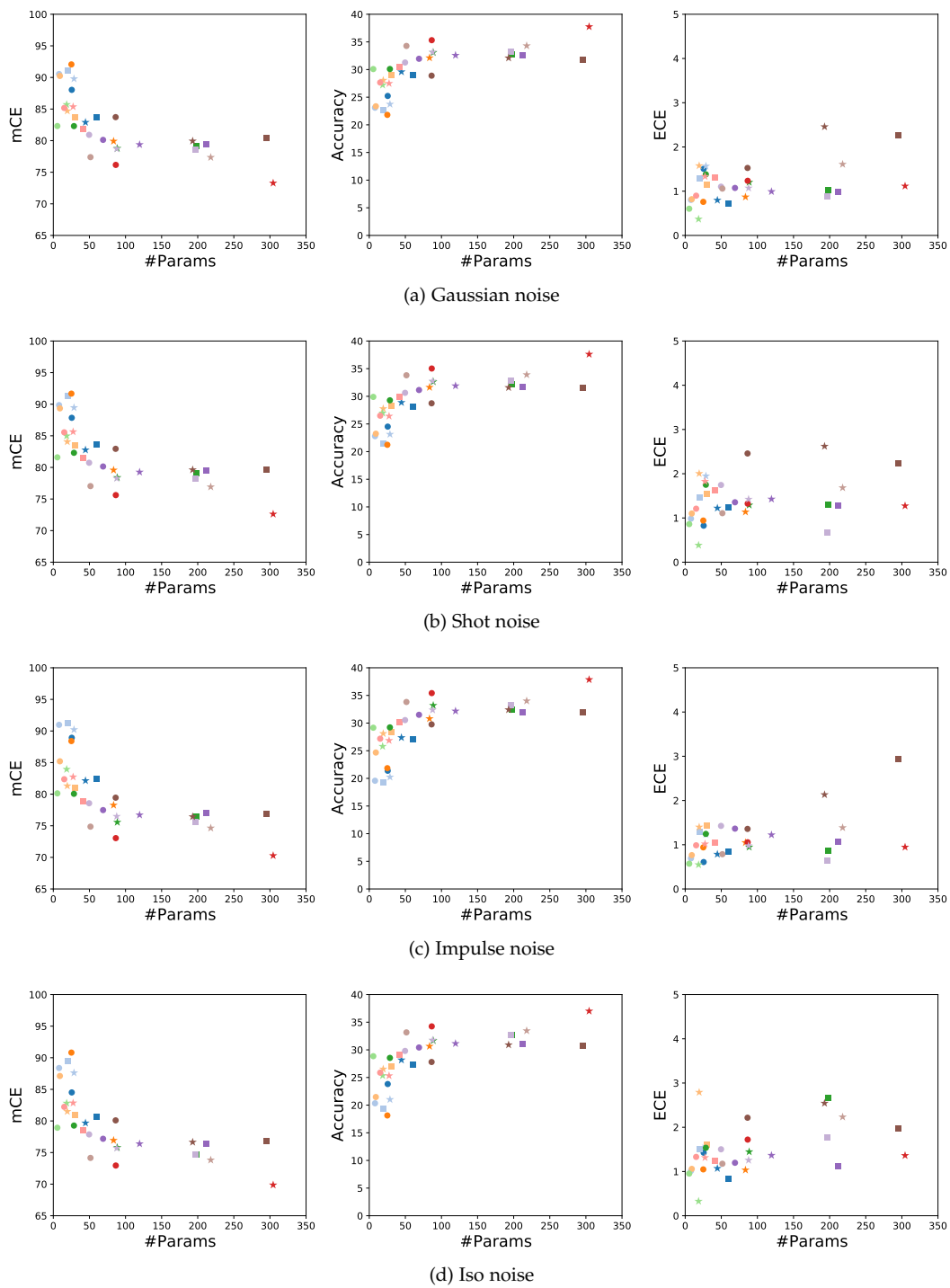


Fig. 10: Detailed performance of pre-trained backbones for noise corruptions (A).

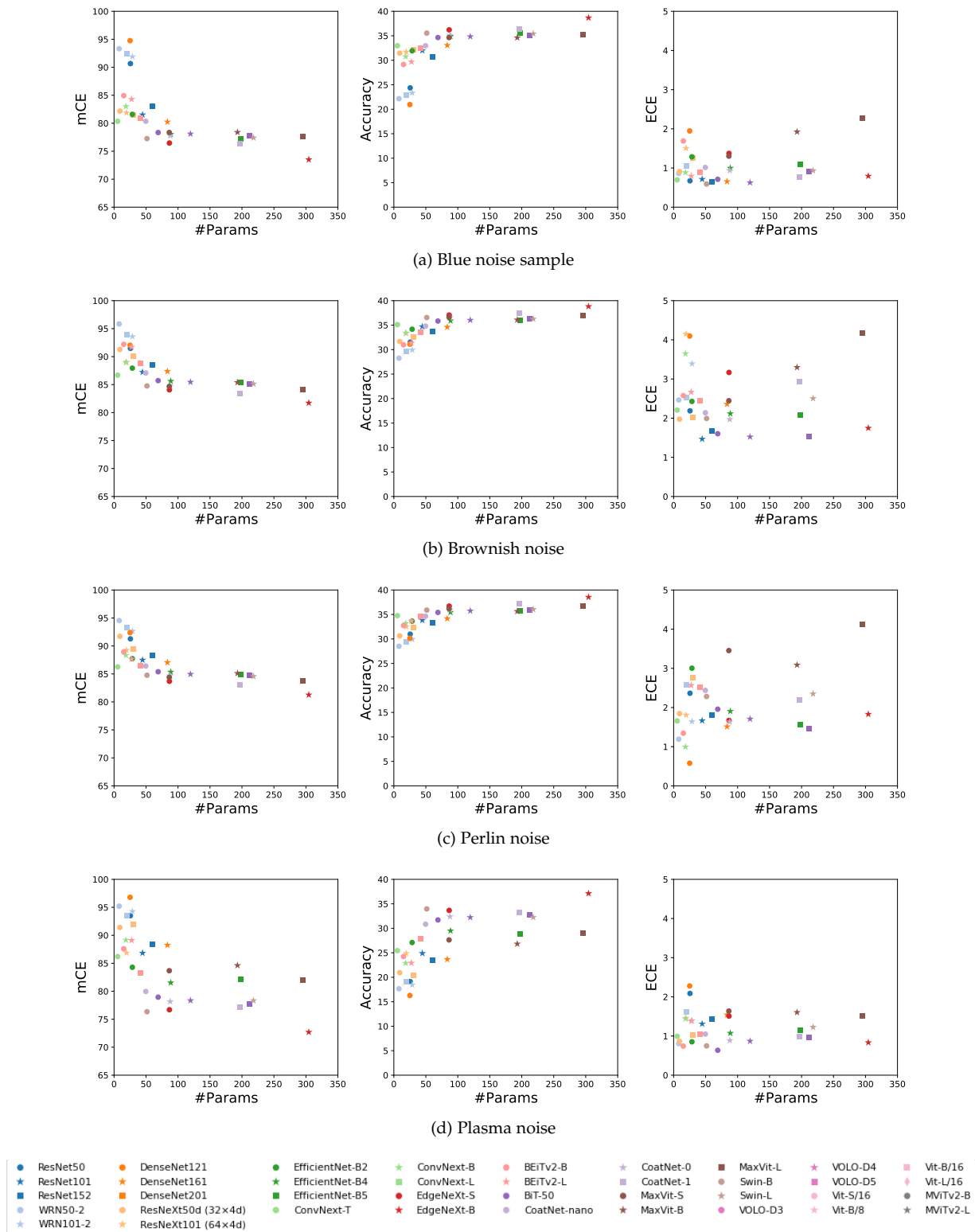


Fig. 11: Detailed performance of pre-trained backbones for noise corruptions (B).

B.2 Robustness against blur corruptions

From Fig. 12 and Fig. 13, we observe that these backbones are in general less robust to blur corruptions than to noise corruptions, highlighted by the higher mCEs, ECEs and lower accuracy. The performance of the models do not differ much in terms of mCEs and ECEs for different blur corruptions. For ECEs across all blur corruptions, the models have more reliable predictions against z-motion blur corruption. This might be because that z-motion blur reserves relatively more information in the center of images, compared to other types of corruption.

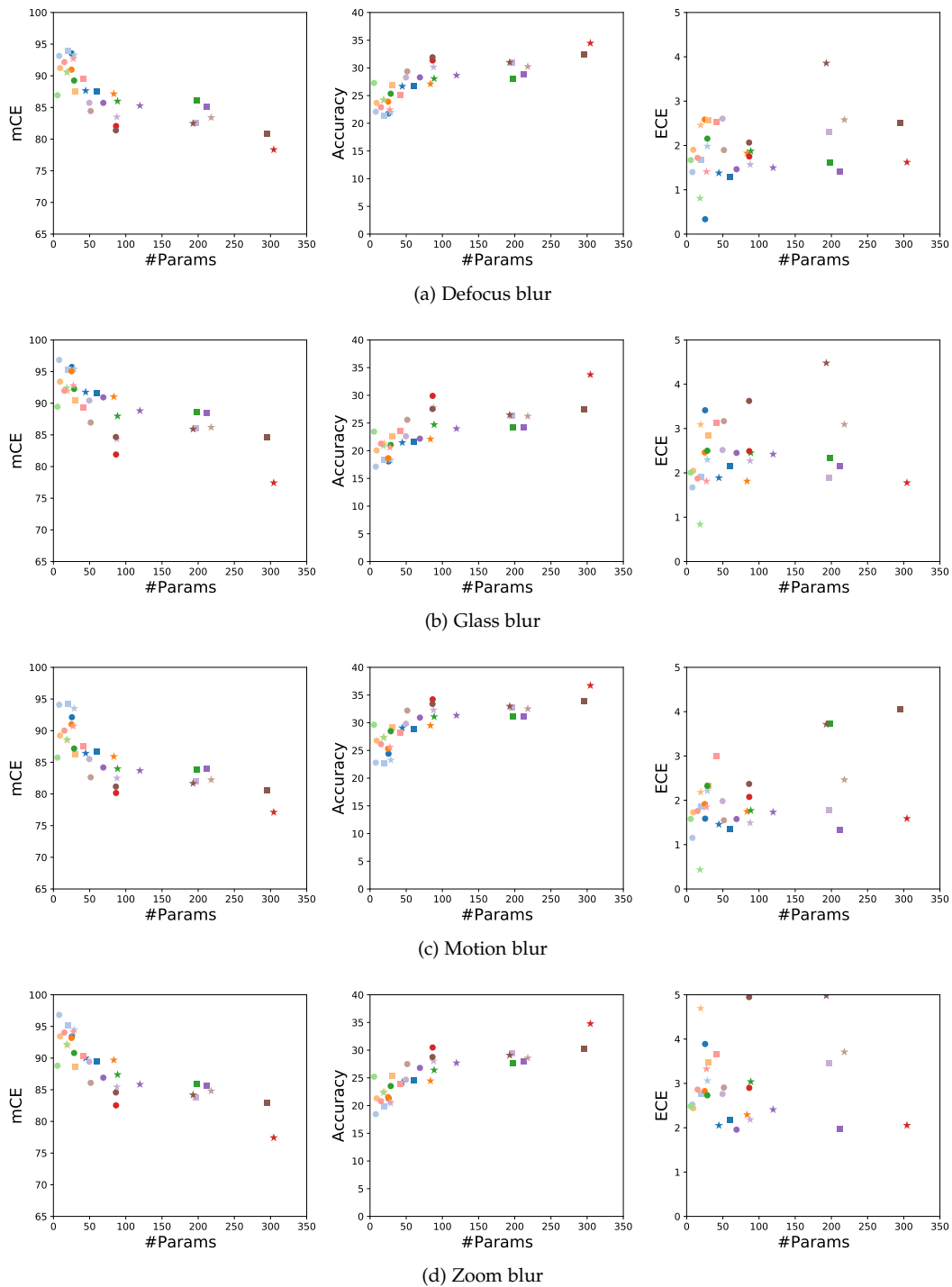


Fig. 12: Detailed performance of pre-trained backbones for blur corruptions (A).

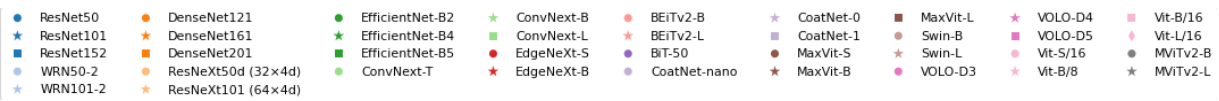
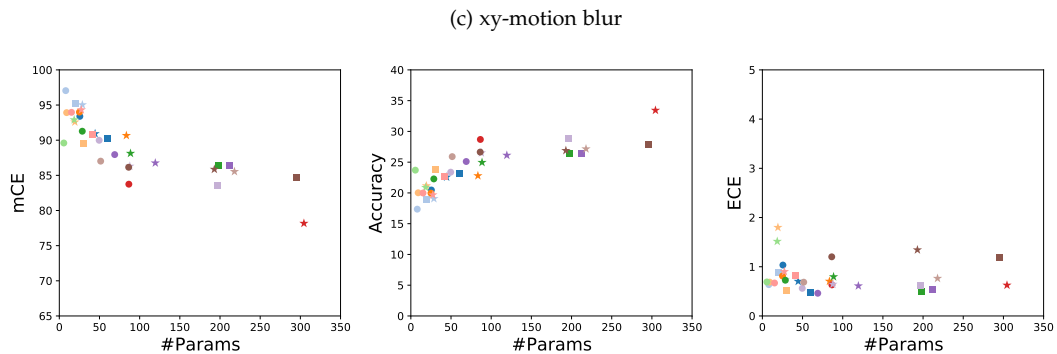
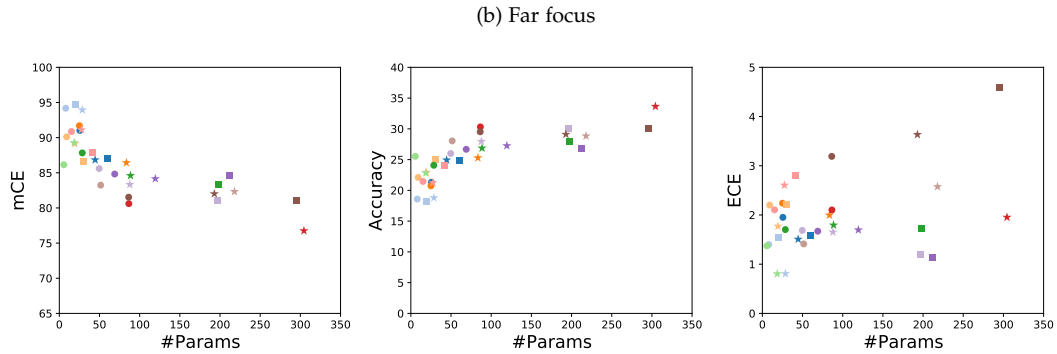
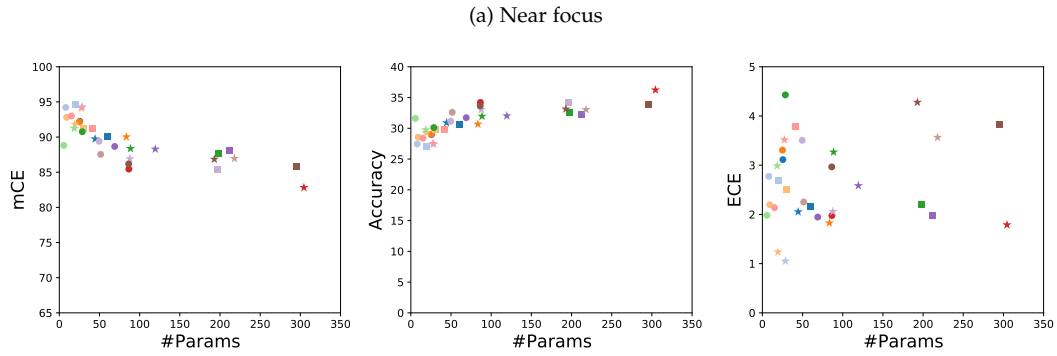
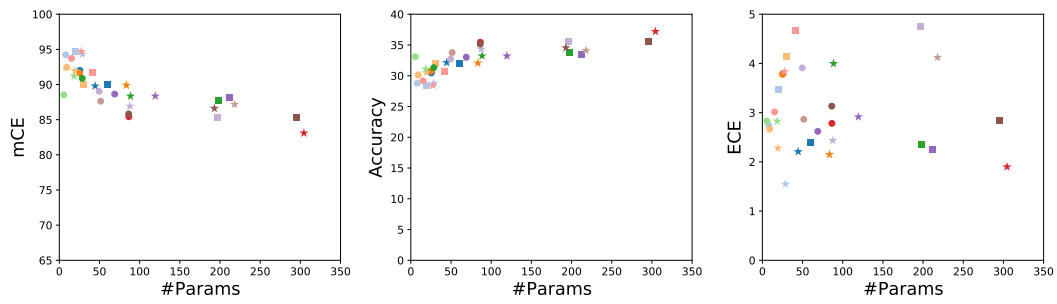


Fig. 13: Detailed performance of pre-trained backbones for blur corruptions (B).

B.3 Robustness against weather corruptions

In Figs. 14 and 15, we observe that the models achieve a much lower ECE on snow and fog-3d corruptions than that achieved on the other corruptions. The differences in mCE and ECE of models against fog and fog-3d corruptions show that considering 3D geometry in the synthetic corruptions is essential to provide a trustworthy and thorough evaluation of generalization and robustness performance of models.

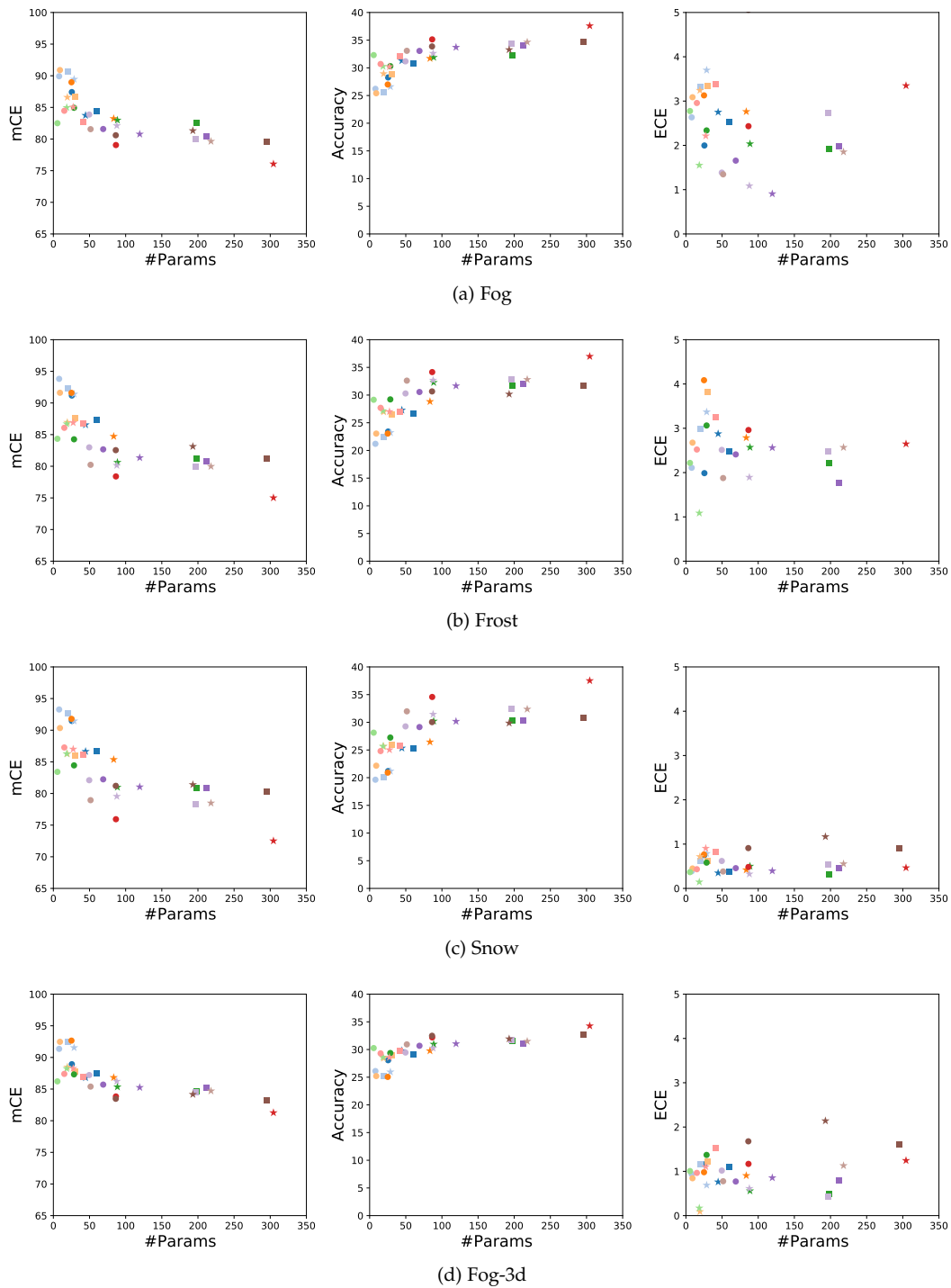
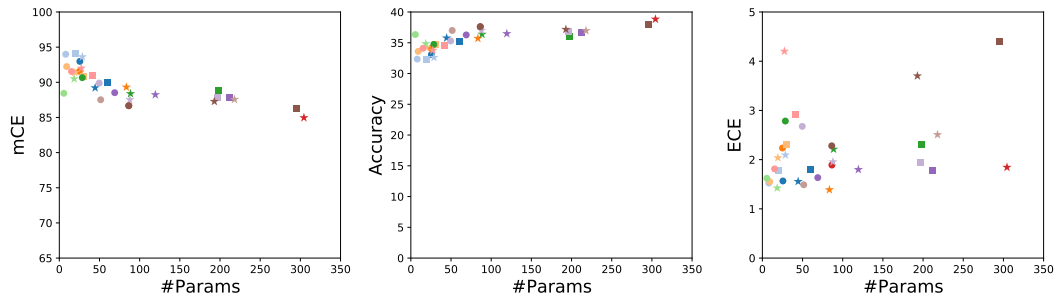
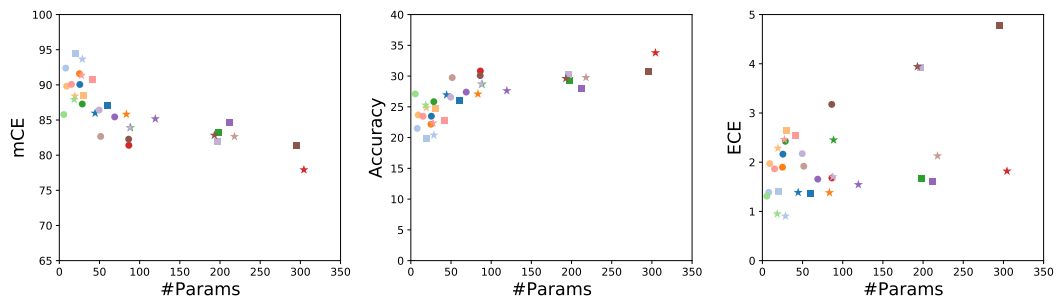


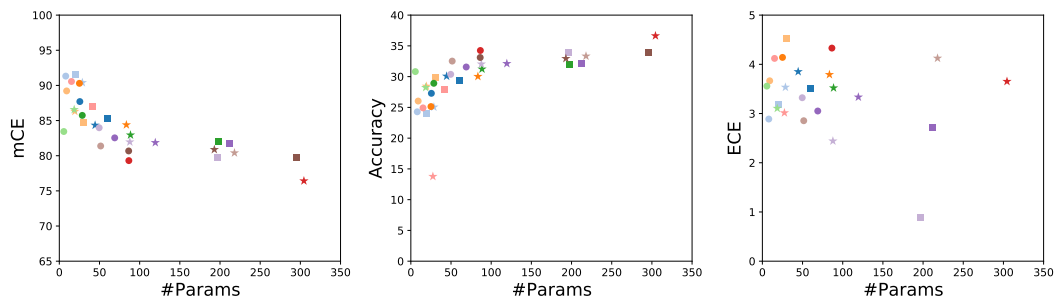
Fig. 14: Detailed performance of pre-trained backbones for weather corruptions (A).



(a) Brightness



(b) Flash



(c) Low light

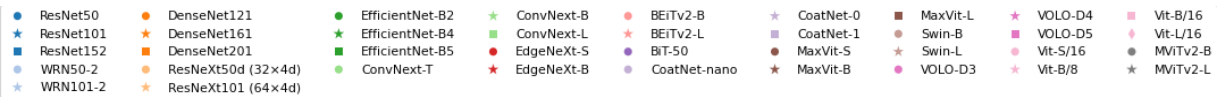


Fig. 15: Detailed performance of pre-trained backbones for weather corruptions (B).

B.4 Robustness against digitization corruptions

From Fig. 16, we observe that, although these models have similar mCEs across all digitization corruptions, they achieve lower ECEs when testing against JPEG compression, h265 abbreviation corruptions, and color quantization. When facing these corruptions, the models can provide more reliable predictions compared to those performed on other corruptions. This is attributable to the fact that the former two digitization corruptions aim at compressing images with as much content reserved as possible, thus visually there are fewer corruption effects than other digitization corruptions. Color quantization preserves much shape information, which can still be used as predictive features for classification.

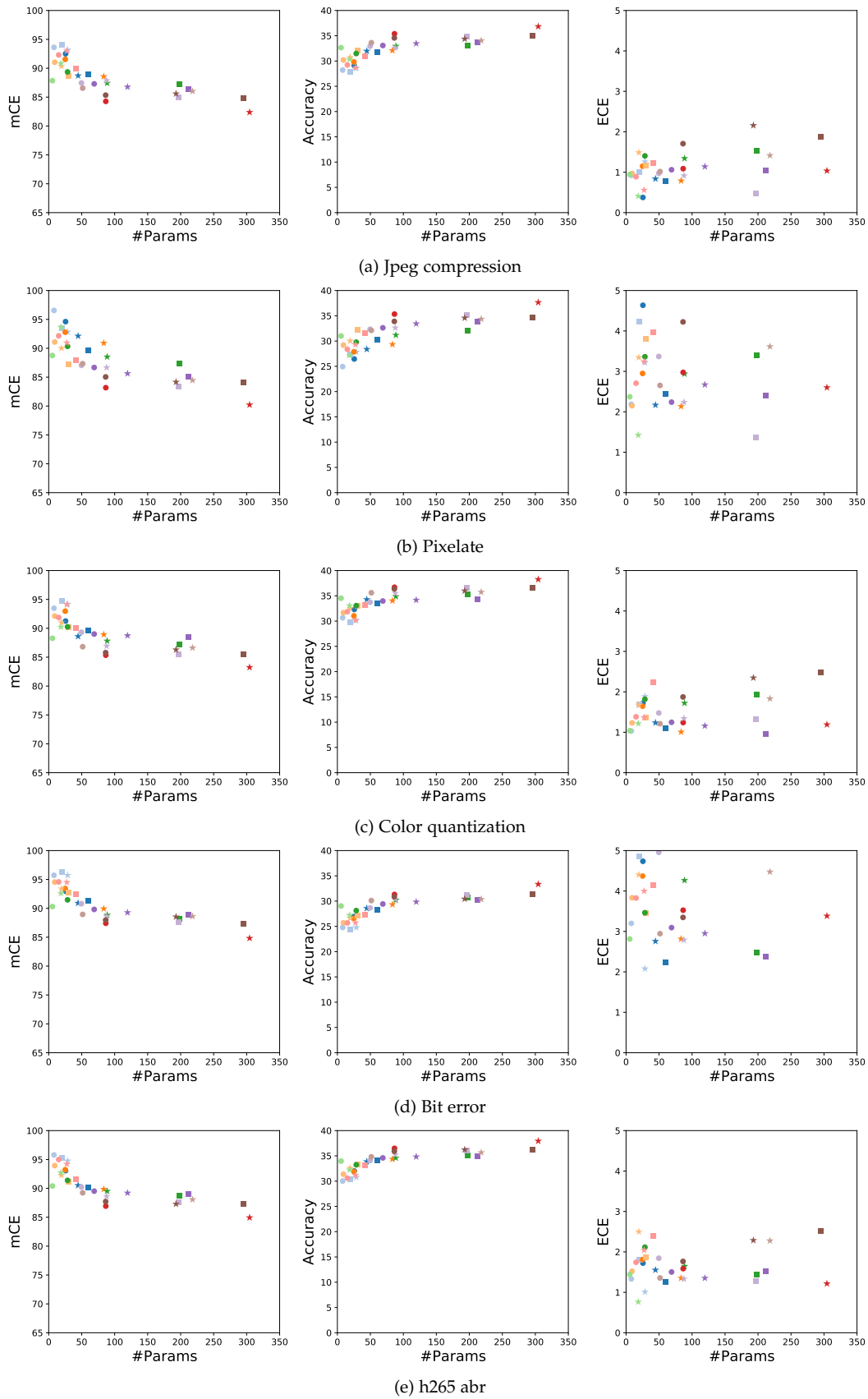


Fig. 16: Detailed performance of pre-trained backbones for digitization corruption.

B.5 Robustness against digital corruptions

In Fig. 17 and Fig. 18 we report the results and comparison of performance of ImageNet backbones on digital corruptions. Transformers demonstrate good robustness to checkerboard cutout corruption, achieving low mCE and high accuracy. Intuitively, we attribute these results to the attention mechanism, which extracts features from input image patches. For concentric sine waves and inverse sparkles corruptions, the robustness of different backbones varies dramatically, especially for large transformers. These two corruptions have strong wave and line patterns respectively, which affects severely the feature extraction from small image patches. Large transformers, e.g. Swin-L and MViTv2-L, are quite robust to single-frequency grayscale corruption. Moreover, although the models have high accuracy toward sparkles corruption, the high ECE values indicate that their predictions are less reliable compared to the other digital corruptions. Sparkle artifacts might overlap with some small patches that contain features benefiting the confidence of predictions, while the lack of these features does not affect much on the accuracy.

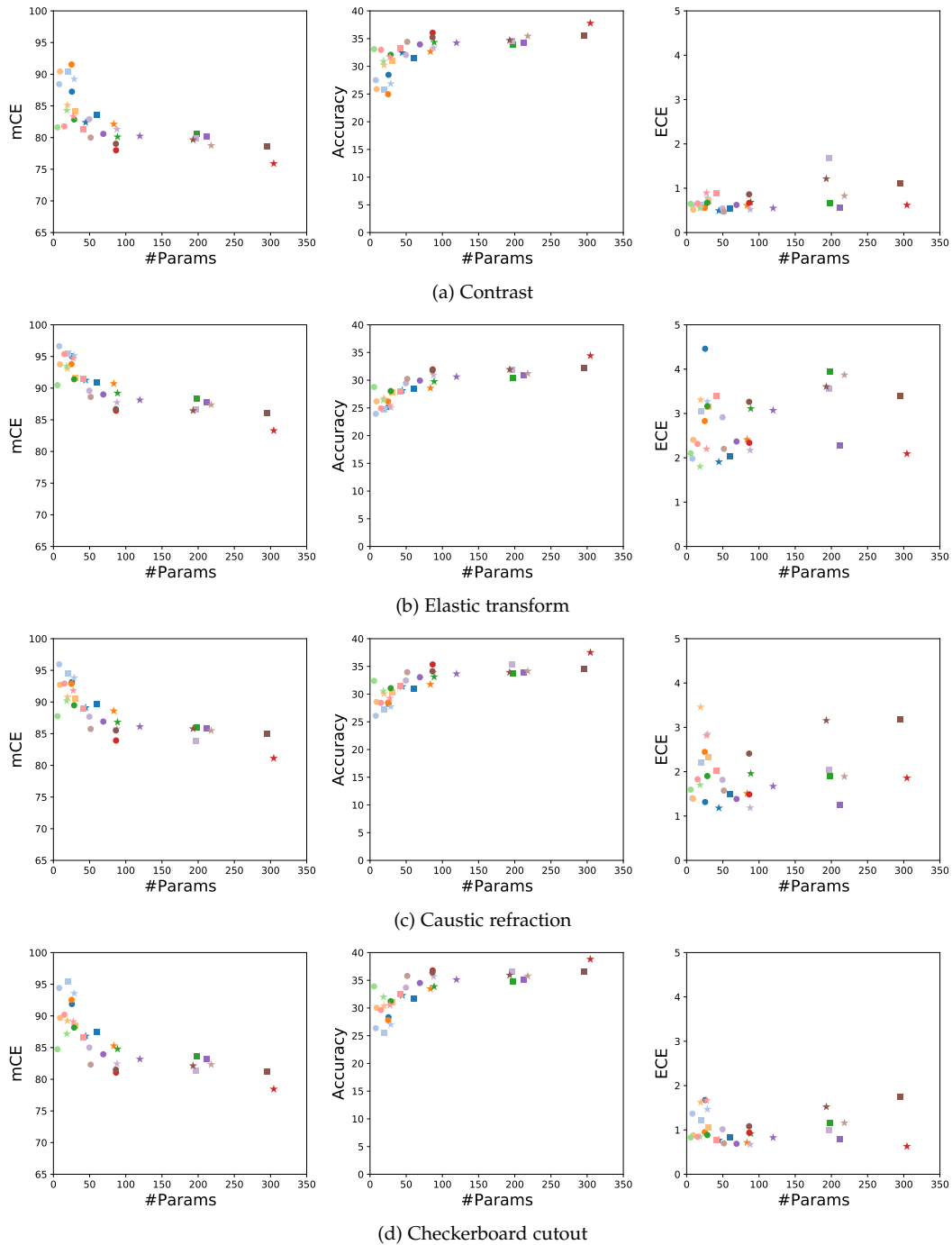
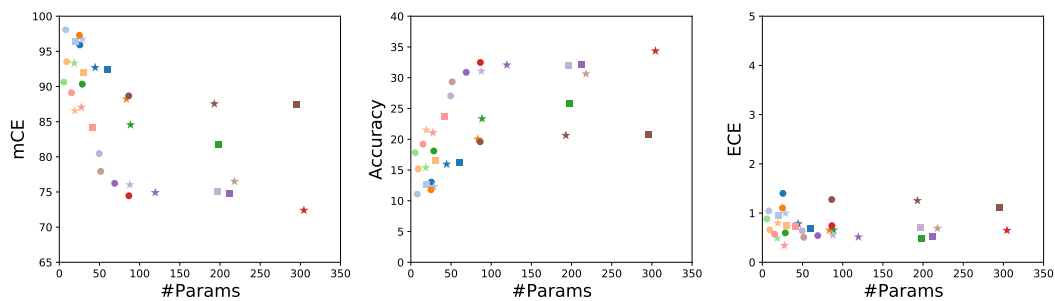
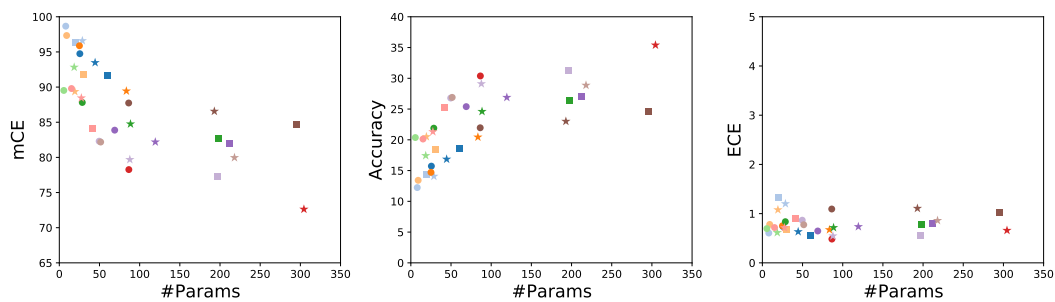


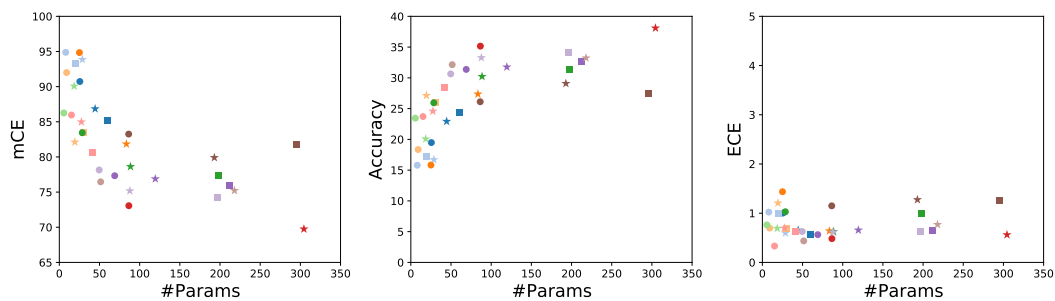
Fig. 17: Detailed performance of pre-trained backbones for digital corruptions (A).



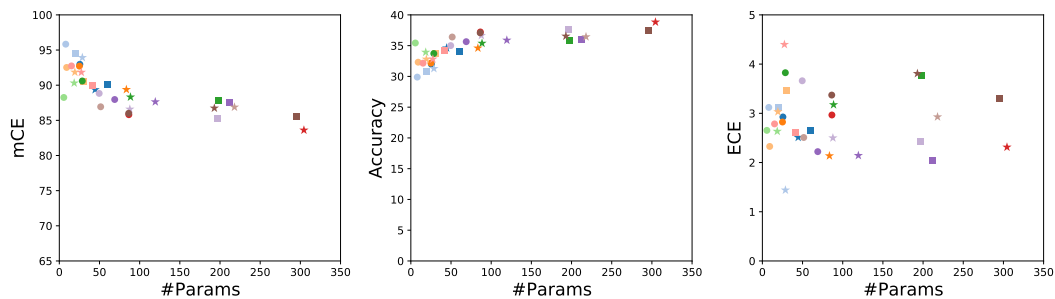
(a) Cocentric sine waves



(b) Inverse sparkles



(c) Single frequency greyscale



(d) Sparkles

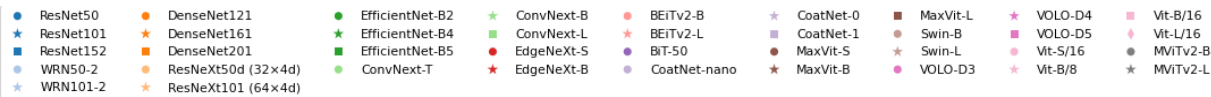


Fig. 18: Detailed performance of pre-trained backbones for digital corruptions (B).